Evaluation of the separation mechanism of the asteroid landing module MASCOT by analyzing test data of a microgravity experiment

Bachelor's Thesis

Author:

Artur Hass

Bremen, 18th of August 2014

Titel:	**Evaluation of the separation mechanism of the asteroid landing module MASCOT by analyzing test data of a microgravity experiment**
	Evaluierung eines Separationsmechanismus für das Asteroidenlandemodul MASCOT anhand aufgezeichneter Daten eines Microgravitationsexperiments
Author:	**Artur Hass**
Matriculation number:	**273399**
First Examiner:	**Prof. Dr.-Ing. Bernd Steckemetz**
Second Examiner:	**Prof. Dr.-Ing. Olaf Frommann**
Supervisor:	**M.Sc. M.Sc. Christian D. Grimm**

Contacts

Hochschule Bremen
Neustadtswall 30
D-28199 Bremen
Phone: +49 421 5905-0

Prof. Dr.-Ing. Bernd Steckemetz
Institute of Aerospace-Technology, IAT
Flughafenallee 10
D-28199 Bremen
Phone: +49 421 5905 5519
Telefax: +49 421 5905 5536
E-Mail: Bernd.Steckemetz@hs-bremen.de

Prof. Dr.-Ing. Olaf Frommann
Institute of Aerospace-Technology, IAT
Flughafenallee 10
D-28199 Bremen
Phone: +49 421 5905 5446
Telefax: +49 421 5905 5536
E-Mail: Olaf.Frommann@hs-bremen.de

Artur Hass
Quintschlag 77
D-28207 Bremen
Matriculation number: 273399
Phone: +49 176 70011046
E-Mail: artur.hass@ingenieur.de
        ahass@stud.hs-bremen.de

German Aerospace Center (DLR)
Robert Hooke-Str. 7
D-28359 Bremen
Phone: +49 421 24420 0

M.Sc. M.Sc. Christian Grimm
German Aerospace Center (DLR)
Dep. of Exploration Systems
Robert Hooke-Str. 7
Phone: +49 421 24420 1266
Telefax: +49 421 24420 1120
E-Mail: christian.grimm@dlr.de

Erklärung

Hiermit versichere ich an Eides statt und durch meine Unterschrift, dass die vorliegende Arbeit von mir selbstständig und ohne fremde Hilfe angefertigt worden ist. Inhalte und Passagen, die aus fremden Quellen stammen und direkt oder indirekt übernommen worden sind, wurden als solche kenntlich gemacht. Ferner versichere ich, dass ich keine andere, außer der im Literaturverzeichnis angegebenen Literatur verwendet habe. Diese Versicherung bezieht sich sowohl auf Text, als auch auf alle enthaltenden Abbildungen, Skizzen und Tabellen. Die Arbeit wurde bisher keiner Prüfungsbehörde vorgelegt und auch noch nicht veröffentlicht.

Declaration

I hereby declare that I have written this thesis without any help from others and without the use of documents and aids other than those stated, and that I have mentioned all sources used and that I have cited them correctly according to established academic citation rules. This declaration applies to the text, all figures, sketch and tables. This thesis is not submitted to any other examination authority jet.

_____

Pace and date   Artur Hass

Abbreviations

CAD	Computer Aided Design
CCS	Capsule Control System
CFRP	Carbon-Fiber-Reinforced Plastic
CNES	Centre national d'études spatiales
CoM	Center of Mass
DLR	German Aerospace Center
DM	Deployment Mechanism
DTC	Drop Tower Campaign
ESA	European Space Agency
FM	Flight Model
fps	Frames per second
HDRM	Hold-Down and Release Mechanism
HY2	Hayabusa2
IAS	Institut aéronautique et spatial
IMU	Inertial Measurement Unit
JAXA	Japan Aerospace Exploration Agency
LM	Landing Module
MAG	Magnetometer
MARA	MASCOT Radiometer
MASCOT	Mobile Asteroid Surface Scout
MESS	Mechanical and Electrical Support Structure
MD	Mass Dummy
MINERVA	Micro/Nano Experimental Robot Vehicle for Asteroid
MUSC	Mascot Umbilical and Science Connector
NEA	Non Explosive Actuator
PRM	Pre-Load Release Mechanism
QM	Qualification Model
S/C	Space Craft
SepM	Separation Mechanism
STM	Structure Thermal Model
WAC	Wide Angle Camera
ZARM	Center of Applied Space Technology and Microgravity

Table 0.1.: Abbreviations

Abstract

In the context of a scientific research mission to an asteroid a small landing system (MASCOT) for measurements on the asteroids surface is examined. MASCOT will be delivered close to the surface with another space craft and will then be descend to perform the mission. Due to the very long communication way and the relatively short life span of the lander, it should be able to fully autonomous cope with its mission. The mission consist of the landing sequence, from the separation of the main ship until the drop down on the surface, the initiation of the mobility function and activation of the different scientific instruments.

Following the first MASCOT Separation Experiment during the 19th DLR Parabolic Flight Campaign undertaken in Bordeaux, France, in February 2012, the second MASCOT Separation Experiment utilized the ZARM Drop Tower in Bremen taking advantage of the close vicinity of the facility and the high grade of achievable Microgravity. During this experiment, conducted in March 2013, an engineering model of the MASCOT Asteroid Lander and an improved separation mechanism was tested for its performance in near zero gravity condition. The separation process is a decisive factor for the outcome of the later mission.

In context of this bachelor´s thesis the separation experiment is analyzed in detail and describes all regarding components and systems.

Contents

List of Figures

List of Tables

1. Introduction and overview

This chapter gives an overview about the Hayabusa2 mission and the therefore developed asteroid lander MASCOT (Mobile Asteroid Surface Scout) with its scientific payload instruments and its support structure.

1.1. Hayabusa2

Hayabusa2 is the immediate follow-on mission to the Hayabusa mission, which returned in June 2010 with the first samples from an asteroid. The target of the Hayabusa mission was the near earth asteroid 25143 Itokawa (1998 SF36). The spacecraft launched on the 9th April 2003 from the Uchinoura Space Center in Kagoshima and arrived at Itokawa on 12th September 2005. During a "Touch-and-go" maneuver soil samples were collected and a Japanese landing module named MINERVA (Micro/Nano Experimental Robot Vehicle for Asteroid) should decent to the asteroid. Due to a timing error the MINERVA lander exceeded the escape velocity and tumbled into space after the rebound. Hayabusa2's target is now the asteroid 1999JU3.
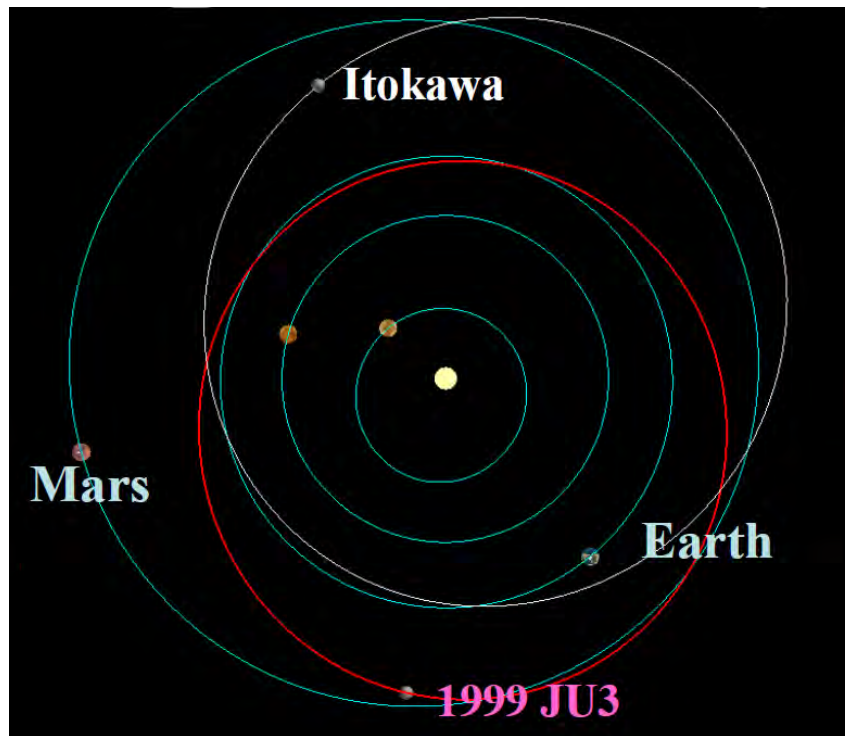
Figure 1.1.: Overview of the target asteroid´s orbits from the first Hayabusa mission Itokawa (white) and the Hayabusa2 mission 1999JU3 (red) [1]

The character of surface is significantly different compared with Itokawa´s. 1999JU3 belongs to the C-Type (carbon) asteroids its surface character is especially similar to the suns and the solar nebula of which the planets arise out of. According to its name is this asteroid characterized by a low albedo (0.03–0.09). The launch is currently scheduled for December 2014 from the Tanegashima Space Center. The spacecraft Hayabusa2 is shown in Figure 1.2 and 1.3. After a four year cruise phase the arrival at the asteroid is foreseen for 2018. Hayabusa2 is equipped with an ion drive, which is characterized by low energy consumption. Subsequent to the arrival at the target asteroid Hayabusa2 will observe the asteroid for about one year from a distance of 50 to 60 km before starting with the primary mission. During a dress rehearsal touch-and-go maneuver MASCOT will be separated which undergoes a slow decent to the surface when it will perform a soft landing. It carries out scientific in-situ investigations and will also provide information to Hayabusa2 to consider the sampling place. In the next step soil samples are intended to be taken by the trunk like looking sampler horn with the aid of a projectile.
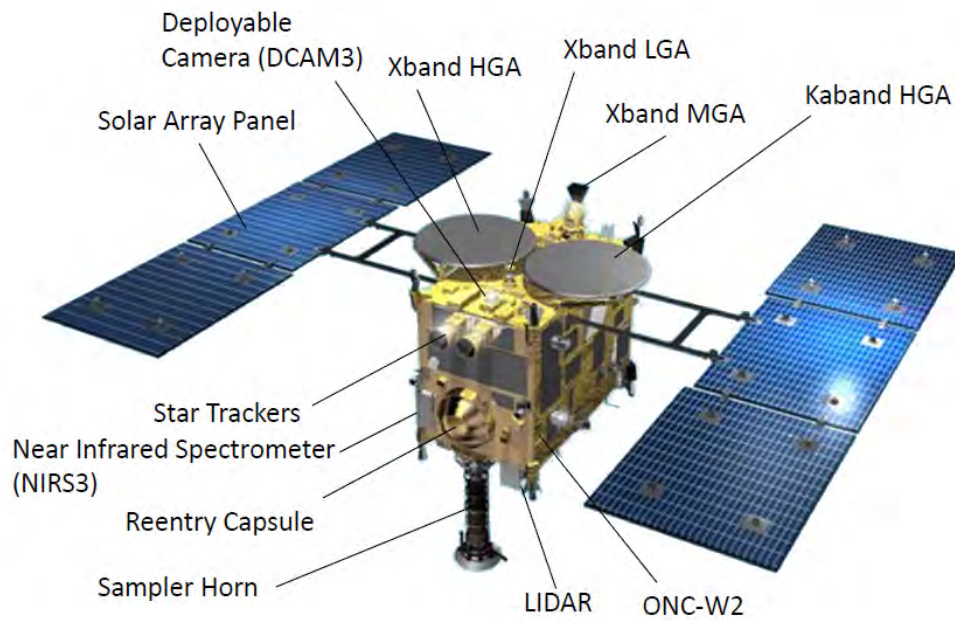
Figure 1.2.: Spacecraft Hayabusa2 with its components in a view from top-front [2]
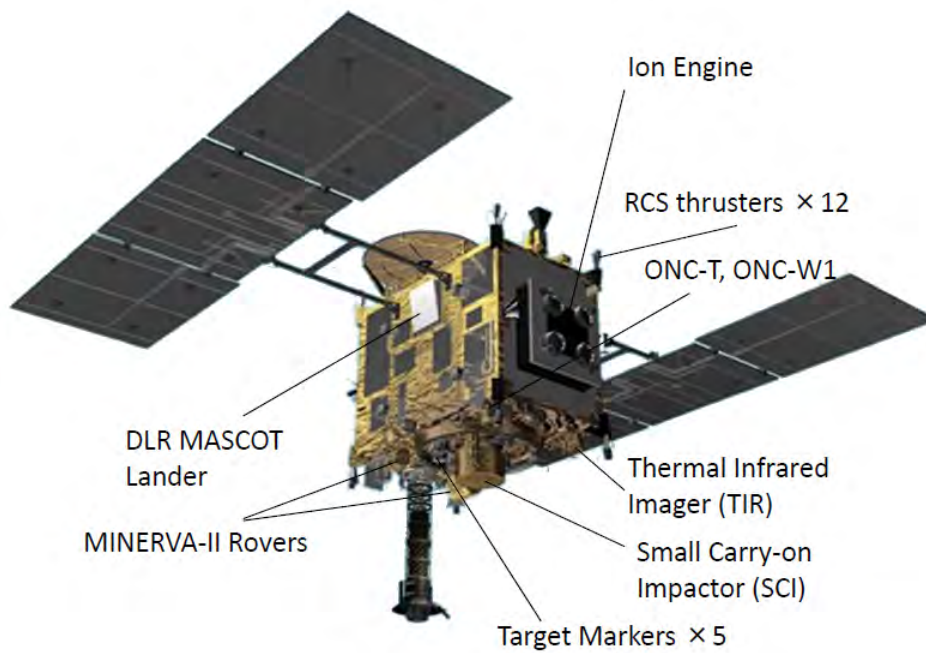
Figure 1.3.: Spacecraft Hayabusa2 with its components in a view from bottom-back [2]

1.2. MASCOT

MASCOT (Mobile Asteroid Surface Scout) is an asteroid lander developed by the German Aerospace Centre (DLR) in collaboration with the French space agency CENS (Centre national d'études spatiales) for the Japanese Hayabusa2-Mission of the JAXA.
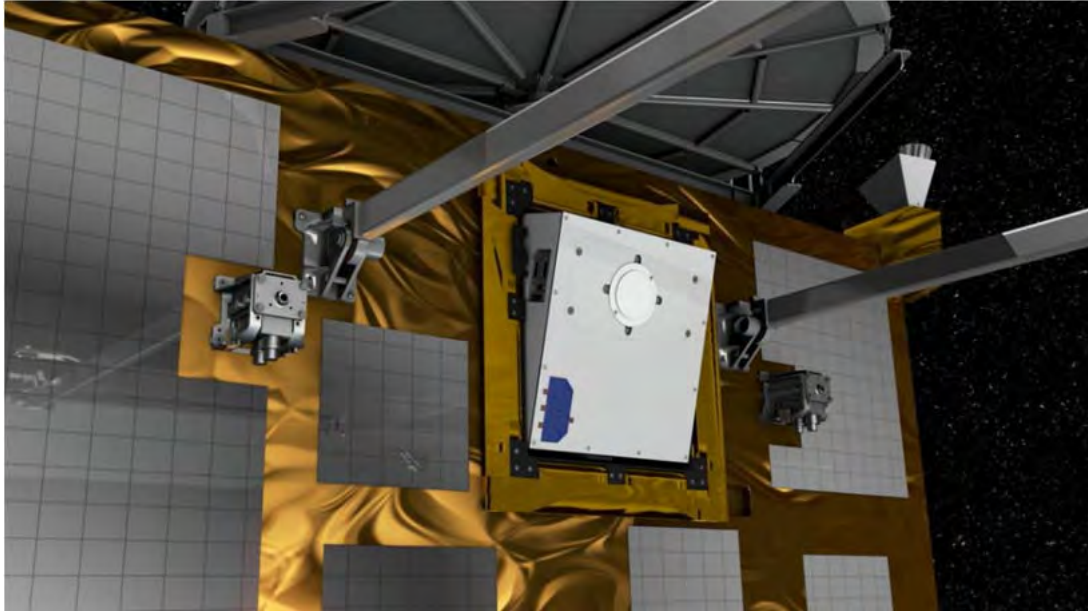
Figure 1.4.: MASCOT in its position in the Hayabusa2 spacecraft

To investigate the chemical composition and physical soil properties of 1999 JU3 in detail MAS-COT will carry out scientific investigation.

Figure 1.5.: Structure of the MASCOT LM

The landing module (LM) has a mass of about 10 kg in which 3 kg are related to the scientific payload. Its structural concept is based on a framework design which consists of a CFRP-foam sandwich design. The foam builds the core which is faced with the CFRP sheets. In Figure 1.5 the MASCOT LM structure is shown.
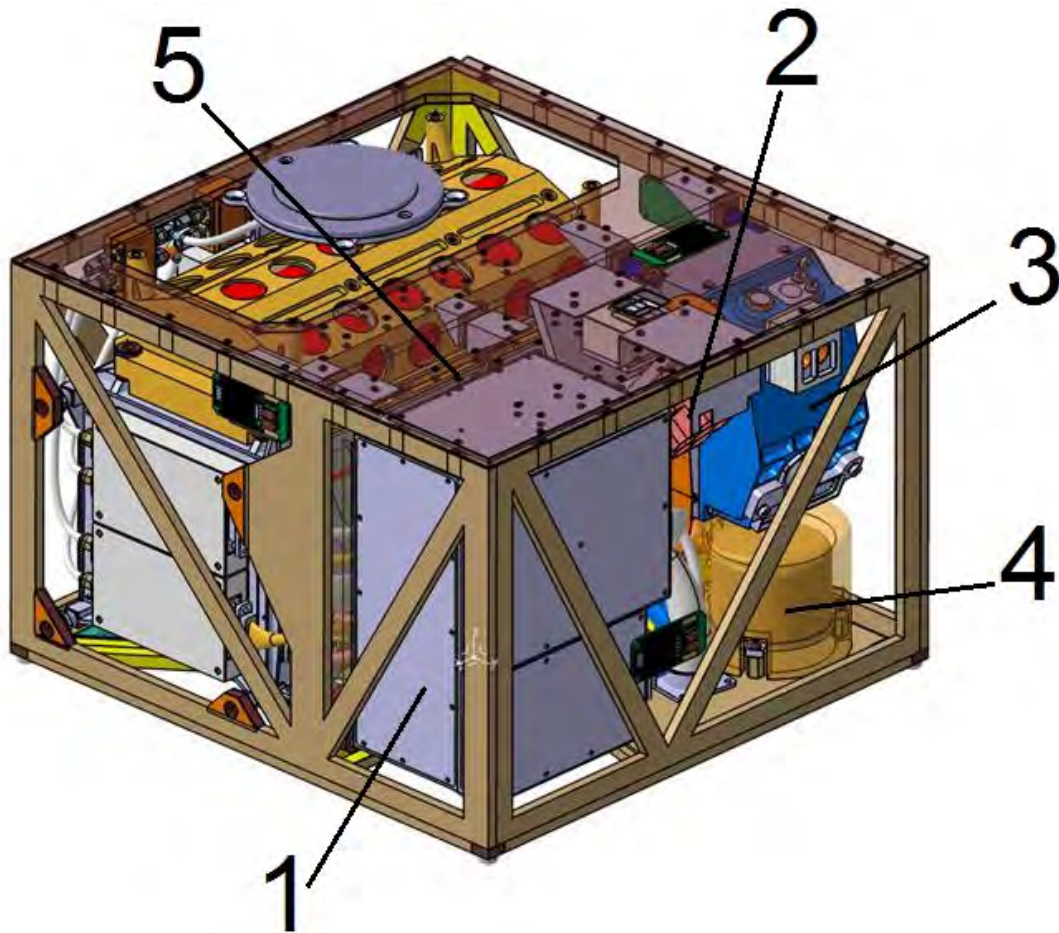
Figure 1.6.: A CAD-model of MASCOT equipped with its instruments (1) MicroOmega, (2)MARA, (3)WAC und (4)MAG

The scientific payload depicted in Figure 1.6 integrated in the LM structure consists of a suite of instruments that are described below.

1. MicroOmega   A near infrared hyper spectral microscope, which is designed to characterize the asteroid surface properties and its composition. It is developed by the French Institut aéronautique et spatial (IAS) and supervised by the space agency Centre national d'études spatiales (CNES).

2. MARA (MASCOT Radiometer)   This is a radiometer which shall detect the temperature, emissivity and heat capacity of the surface. It is developed by the DLR Institute of Planetary Research (Berlin).

3. WAC (Wide Angle Camera)   It shall take panchromatic high resolution images of the landing site. To enable a operation during the night phase, the WAC is equipped with LED illumination. Secondly, the images will be provided to the MASCOT Autonomy Manager which is process the data for relocation. It is although developed by the DLR Institute of

Planetary Research (Berlin).

4. MAG (Magnetometer)   The magnetometer shall measure the magnetization of the asteroid if it exists. It is developed and manufactured by the Technical University Brunswick.
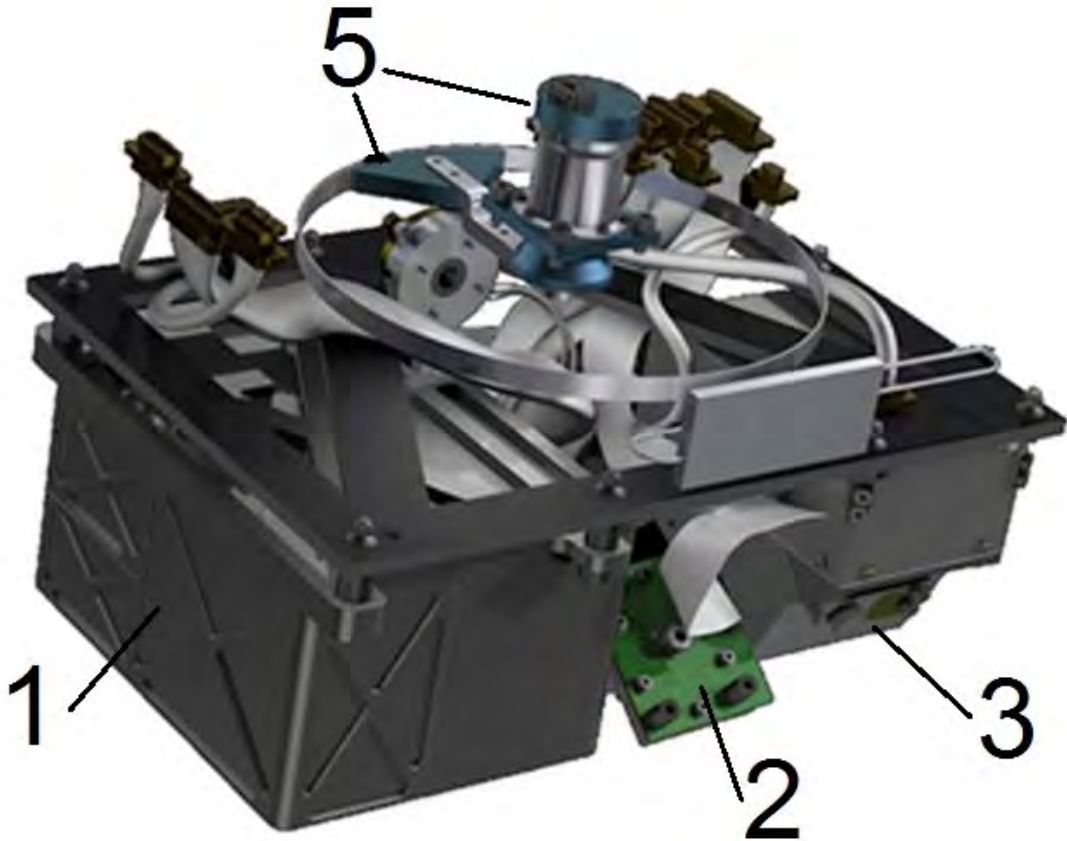
Figure 1.7.: Rendered picture of MASCOT's payload and the mobility mechanism

Mobility (5)   Furthermore MASCOT is equipped with a unique Mobility Mechanism, which is made up of an electric motor and an eccentric mass mounted on an arm. The Mobility has two main tasks.

- Upright the LM after landing if required
- Relocation by hopping maneuvers to enable measurements on different sites

A more detailed view is given in figure 1.7. The Mobility is developed by the DLR Institute of Robotics and Mechatronics.

After a successful separation, descending and landing on the asteroid surface operational scenario of MASCOT will be started. It foresees two hopping and up-righting operations within only 16hrs (two full asteroid day / night cycles) service life. Due to the short lifetime on the asteroid´s surface it is foreseen to conduct all surface operations autonomously, without any intervention from Earth. Figure 1.8 shows the sequence of MASCOTS´s mission scenario.
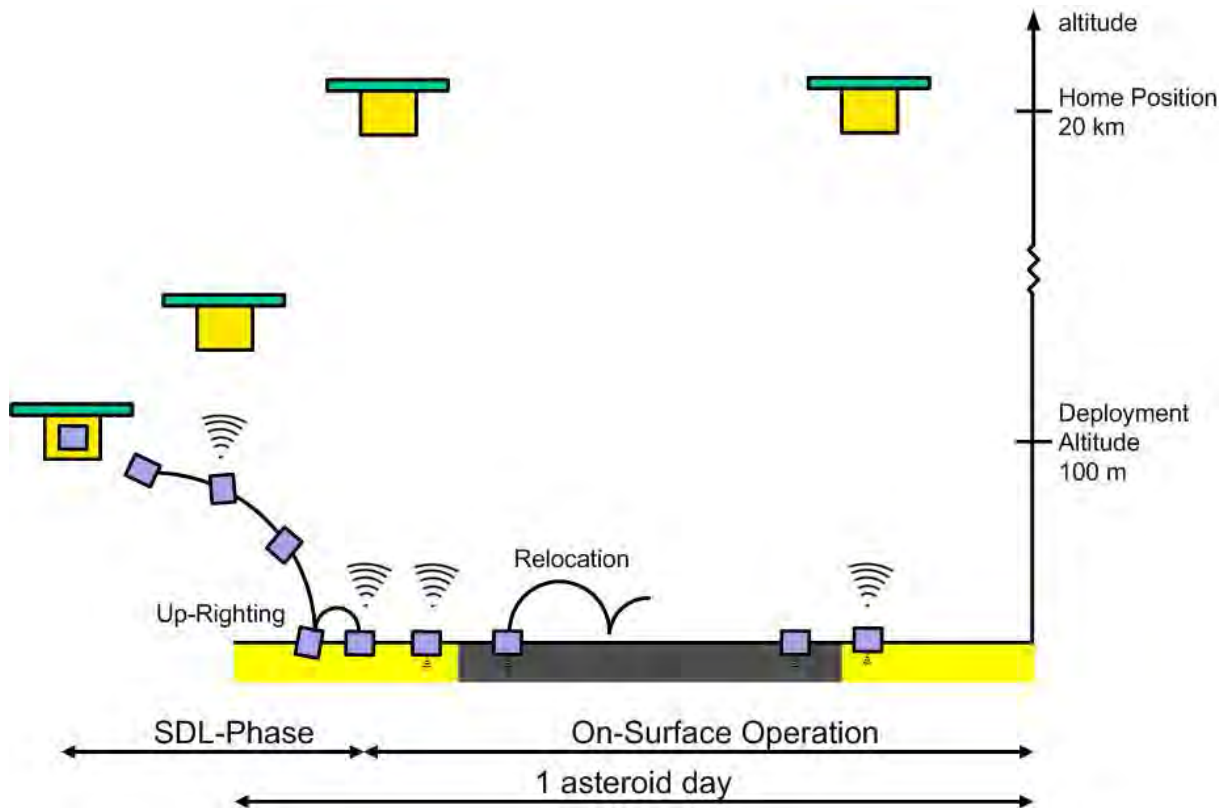
Figure 1.8.: Sequence of the MASCOT mission scenario [4]

After landing, MASCOT will first seek to establish it's attitude, and then perform any necessary reorientation maneuvers. MASCOT will than start the scientific operations and send the collected data to Hayabusa2 just during daylight. On the second day MASCOT will upload the data from the previous night and then start the relocation maneuver. This will involve a first hop of several tens of meters, followed by shorter reorientation maneuvers to bring the payloads back to the correct orientation to local ground. The science operations will then start again at this second location.

Under current assumptions, it seems likely that MASCOT´s energy will run out before the second night. If not, science operations and a possible second relocation will be performed, until the energy is depleted.

For a successful mission relating to MASCOT there are two critical phases:

- Separation from the main spacecraft
- Soft touchdown on the asteroid surface

The separation experiment which took place in March 2013 at the location of the Center of Applied Space Technology and Microgravity (ZARM) in the Drop Tower Bremen was addressed to investigate the first critical stage.

1.3. MESS

This descriptions were taken from several literature sources [3], [4].

MASCOT will be accommodated during the cruise phase in the so called Mechanical and Electrical Support Structure (MESS). The MESS is attached to Hyabusa2 on its side face (figure 1.4) to the so-called HY2-Y-Panel and acts as an interface between the MASCOT LM and the main spacecraft Hayabusa2.

Figure 1.9.: Mechanical and Electrical Support Structure (MESS) for the MASCOT LM

The MESS structure has the followed functionality:

- It acts as interface structure for MASCOT LM and is thus the main load bearing element between LM and the Hayabusa2 structure.

- It thermally insulates MASCOT from the Hayabusa2 spacecraft and closes the MASCOT dedicated cut-out in Hayabusa2-plane during return phase.

- The Push-off Mechanism is supported by the MESS and pushes LM away after releasing an actuator.

- A single Umbilical Connector is the electrical interface between HY2 main-S/C and MASCOT during the launch and cruise phase.

- It provides an interface for the MARA/WAC calibration target.

Its location and position at the HY2-Y-Panel is shown in detail in figure 1.10. The inclined position of MASCOT in reference to the HY2-Y-Panel by an angel of 15° is caused to prevent a collision of the LM with HY2´s solar panels.
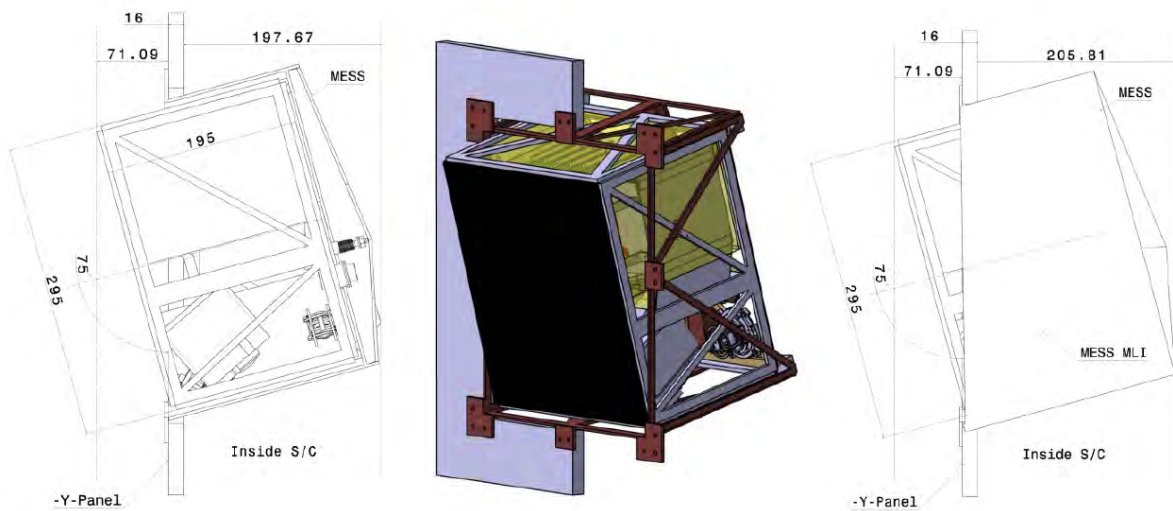
Figure 1.10.: Integrated MASCOT LM with the MESS in the HY2 –Y-Panel[4]

The structural concept of the MESS is based on a framework design as depicted in Figure 1.9. Except of the main truss in the top middle all other struts are made up of solid high modules carbon-fiber-reinforced plastic (CFRP) unidirectional prepreg plies. The main truss consists of a CFRP-foam sandwich construction. The core is made of a Rohacell IG-F 31 foam which is faced with CFRP sheets.

Between the MESS and the LM are six contact points which are shown schematically in figure 1.11. This points are four cup-cone shaped stand-off elements in the corners, a non-explosive actuator (NEA) and a push off mechanism.
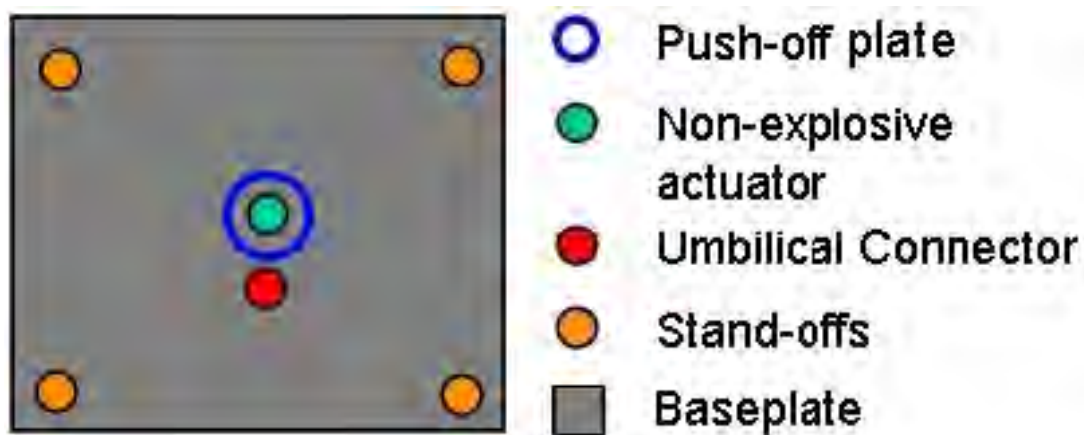
Figure 1.11.: Schematic principle of MASCOT to MESS contact points[4]

Direct contact between MESS and LM is realised by metallic Stand-offs located in all 4 bearing

corners between the composite structures. The MESS Stand-Offs have a conic base shape on their inner surface, whereas the opposite LM´s Base Plate Stand-Off have a small radius. This design allows a certain self-centring and tilting of the LM when it is pulled into the MESS. Additionally the MESS Stand-Off has a collar which prevents LM of moving further horizontal direction after "leaving" the conic shaped mould. A detailed sectional view of a CAD-model is given in figure 1.12.
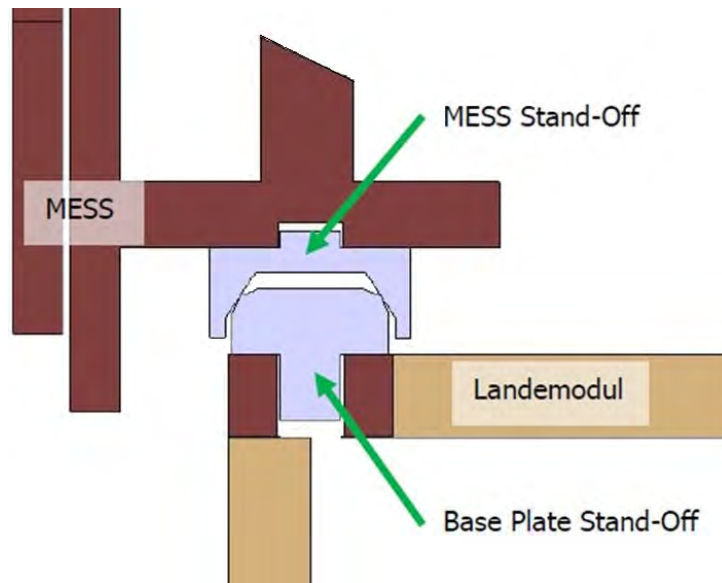
Figure 1.12.: Detailed sectional view of the stand-offs and the bearing corners

Both sides stand-offs are glued to their corresponding structure. Though, the position is mainly ensured by form fit (bolt extension) and pull forces of the centric NEA bolt. To ensure contact in the cup-cone elements during the launch phase there is a pull force of a value of 2500 N required. On the other hand a smooth release of the LM towards the asteroid has to be guaranteed as well. In the early project phase multibody simulations and early tests showed that this value has to be significantly lower than 1000 N. A force in the order of 200 N was figured out as a common value.

2. Scientific Background

This chapter gives an overview of similar mechanisms which were used on former missions and the development evolution of MASCOT's separation mechanism at DLR. Furthermore it subscribes the actual design.

2.1. Mechanisms

This descriptions were taken from several literature sources[5], [6]

To hold the appendages of spacecrafts in their position during launch and cruise phase and later to deploy them in their actual operating position or orbit specific mechanisms are used. This appendages can be booms, solar arrays, antennas or sub-spacecrafts like satellites or lander which can be payloads for a main-spacecraft or a main-ship. To fit this appendages in a given volume or to held them down to prevent a damage during critical phases.

In general there are two different types of mechanisms to achieve this attributes, the hold-down and release mechanisms (HDRM) and the deployment mechanisms (DM).

- Hold-down and release mechanisms are off-the-shelf components and commonly used in spacecraft to fulfill critical tasks. The basic functions of a HDRM are to hold down and to secure during launch and cruise phase and to release once the operation of the deployable, separable or moveable payload or appendages is required.

- "Deployment mechanisms are used to enable deployment of a released appendage from its stowed position to its operational position following a defined set of kinematics and passive-to-active controlled dynamics. Once the final position is reached, the appendage is either latched at a defined position or the DM is used as a re-pointing or trimming device in order to achieve specific mission related functions." [5, 230]

Hold-down and release mechanisms are used commonly in conjunction with deployment mechanisms. In some special cases HDRMs can not used in context with DMs.

Regarding hold-down and release mechanisms applied in spacecraft can separate in three functional parts.

- Hold down preloading assembly: This part secure the device in stowed configuration during launch and cruise phase and provides the required preload. It can be e.g. a rod, cable, bolt or nut.

- Hold down release actuator: "It achieves the release of the preload upon the command of a drive electronic. The release actuator is generally mounted on the fixed part of the separable interfaces. Its also frees and secures the separable interfaces from any mechanical links and, prevents any interferences upon deployment or operation of the appendage. For some applications, the bolt or threaded rod is ejected upon release and secured into a so called bolt catcher via a dedicated spring and/or thanks to the stored strain energy." [5, 230]

- Hold down load carrying structure: "It guarantees the launch loads transmissibility between the fixed part and the part to be released. This element completes the HDRM assembly and is always adapted to each appendage and spacecraft interface." [5, 230]

2.2. Evolution of MASCOT Separation mechanism

From the beginning of the project, with the aim to develop a lander with a mass of about 10 kg and the relative small dimensions, it was clear that MASCOT won't have any thrust generating or altitude control systems. After the decent from Hayabusa2 it has to decent down on a ballistic path to the asteroid.

The first ideas were to choose an actuator for MASCOT's separation which works after the pin pullers principal. Before a release occurs the holding pin respectively rod is pulled until a specific stress inside the rod leads to a intended failure. This leads to the problem that the preload raises before separation takes place. Due to the raise of the preload MASCOT will be flipped out uncontrolled of the MESS. A smooth separation and a low enough separation velocity can not achieved by this solution.

By this awareness a hold-down and release mechanism, precisely the SSD9100 from NEA Electronics was chosen.

The evolution of push-off plate leads to its characteristic V-shaped form. The early push-off plate design based on a flat LM surface. The change in the LM structure to a framework design lead to the change of the push-off plate design. In figure 2.1 is an early design of the separation mechanism with a round push-off plate depicted.

The design which is state-of-the-art at the DTC is shown in figure 2.2 and 2.3.
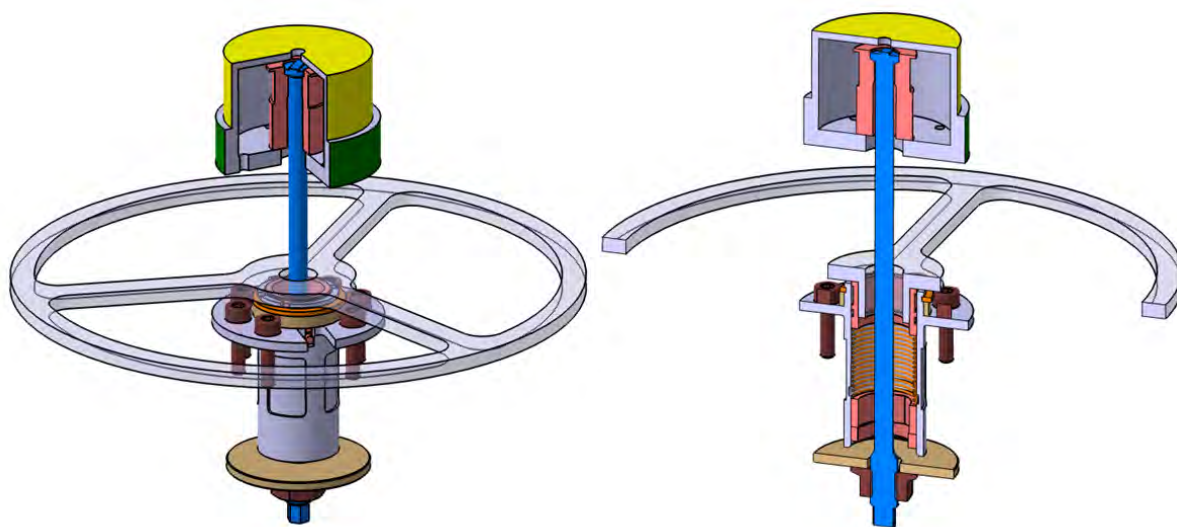
Figure 2.1.: Early design of the SepM with a round push-off plate

2.3. MASCOT Separation mechanism

2.3.1. Principle of function

When the actuator releases MASCOT from its position in the MESS, a compression spring drives a push-off plate which pushes MASCOT into its eject trajectory. The energy stored in the compressed spring corresponds to MASCOT´s required ejection velocity of 0.05 m/s.
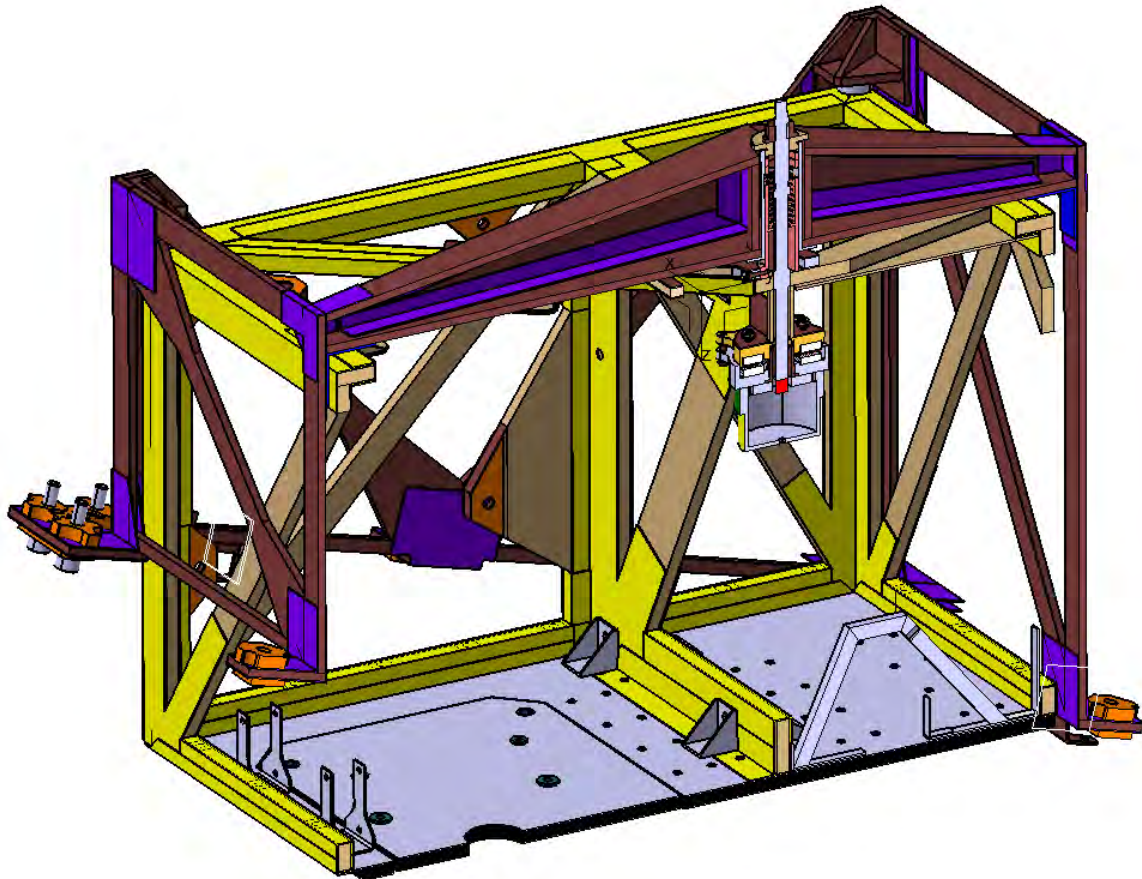
Figure 2.2.: Mascot mid-plane section showing the position of the SepM inside the Landing Module
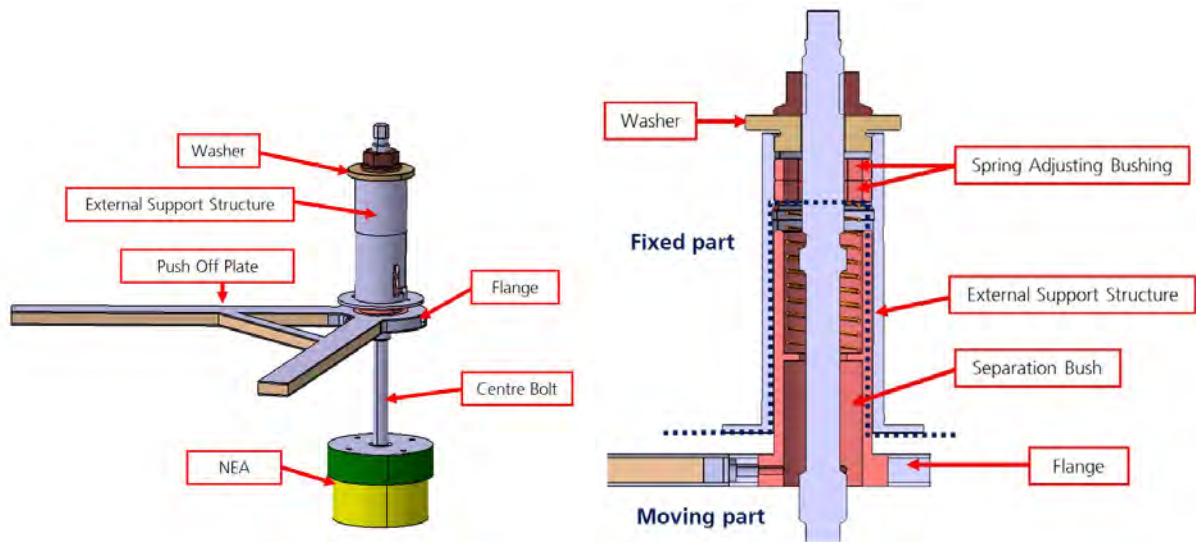
Figure 2.3.: Left: Overview of the Push-Off Mechansim including push-off plate and the NEA
Figure Right: Section through the push-off mechanism

The external support structure is placed in the MESS main truss and fixed with a washer on its top and a small collar at bottom side. Within the external support structure, placed between the fixed and the moving parts, is the separation spring. When the MASCOT Landing Module is installed in the MESS the spring is compressed. At separation, the spring pushes the moving part of the Push-Off Mechanism and thus the MASCOT Landing Module away from the MESS.

The Push-Off Plate is of CFRP-foam sandwich, 4.5 mm in thickness. At the interface to the separation bush the foam is replaced by an aluminum flange which provides the interconnection. The Push-Off Plate is shaped to fit on the struts of MASCOT landing module. The purpose of the Push-Off Plate is to distribute the pushing force on the landing module so that rotation during separation can be prevented even though the CoM is not in the axis of the Push Off Mechanism.

2.3.2. Non-Explosive Actuator

The information and description in this chapter was taken from [7]

The non-explosive actuator (NEA) SSD9100 which acts as a HDRM for MASCOT is an electrically initiated, one-shot release mechanism. It is produced by NEA Electronics,CA,USA and shown in figure 2.4. This and similar mechanisms from NEA Electronics have flight heritage on several space missions. On the ESA mission Rosetta it will be used to release the lander Philae.

Figure 2.4.: Non explosive actuator (NEA) SSD9100

The preload is applied through the main bolt that is held in place by two separable spool halves which are in turn held together by tight winding of restraining wire.

It requires an actuation current by the spacecraft. An umbilical electrical connector provides the electrical interface between MASCOT and the MESS and provides a switch as feedback signal line to indicate MASCOT´s separation upon opening of the umbilical. The restraint wire unwinds allowing the spool halves to separate releasing the main bolt and the preload.

The function is shown in figure 2.5.

The principle of operation involves a tensile load reacting against a spring-wound split spool.

Upon fuse wire initiation the spring unwinds. This allows the spool halves to separate.

Releasing the tensile load slowly to minimize the release of strain energy and therefore minimizing shock.

2 amp min.

Preload

Preload

Ejection
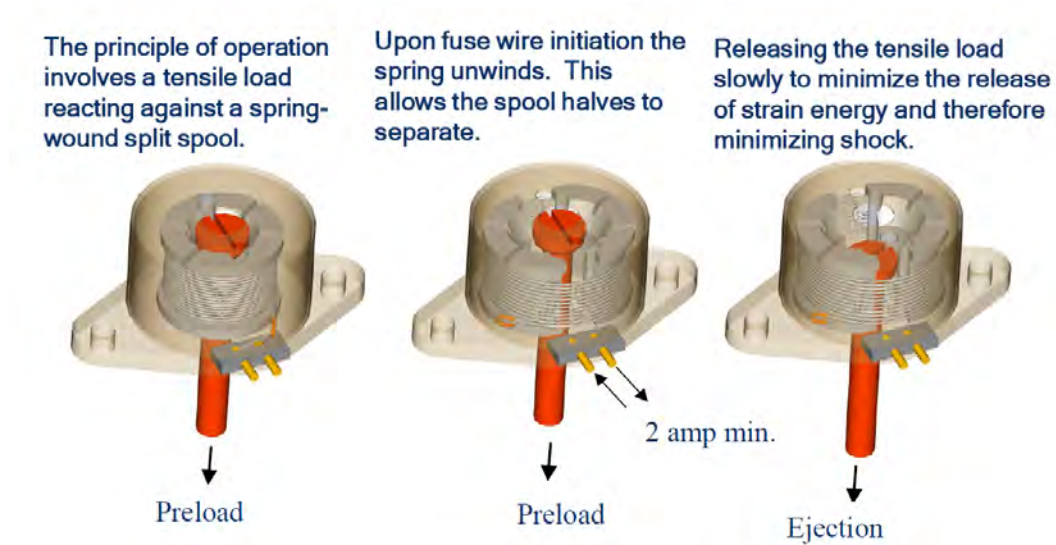
Figure 2.5.: NEA functional principle [7]

The NEA fulfills two functions:

- The load bearing/transmission, i.e. keeping the bolt, which connects MESS and MASCOT LM, in its rest position on the LM's side.

- Releasing MASCOT at the deployment position above the asteroid surface, triggered by a main-spacecraft command. The separation command (1 nominal trigger channel and 1 alternate channel) closing the igniter box's NEA nominal ignition channel or alternate channel respectively. A fuse current of 3 A is provided to the NEA´s fuse. This actuation logic is depicted in Figure 2.6.

3A

3A

60ms

Separation Command

IG Box

Non Explosive Actuator

Fuse 1

Fuse 2
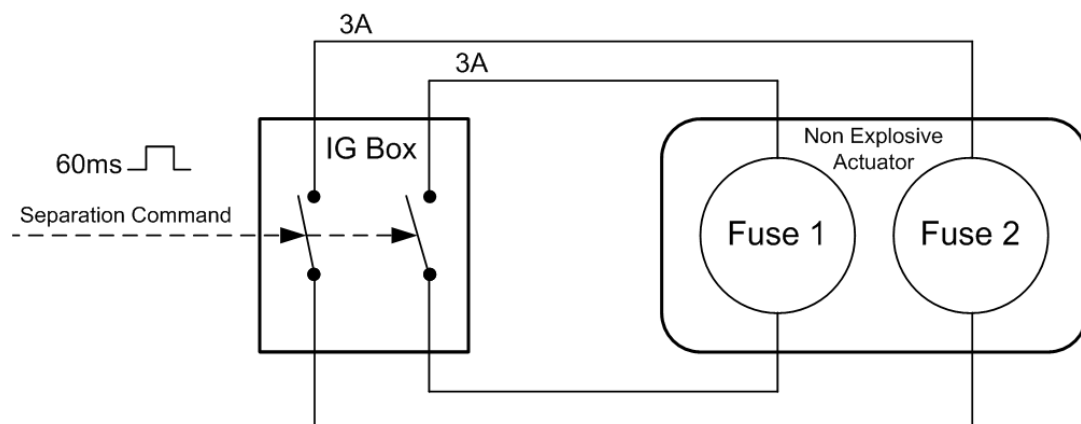
Figure 2.6.: NEA actuation schematics [4]

A plot of the strain energy release which is provided by NEA ELECTRONICS is shown in figure 2.7 for a SSD9101B. The nominal values are not corresponding to MASCOTS´s use but the graph characteristics are similar and correlated with the results of the test in a later chaper.
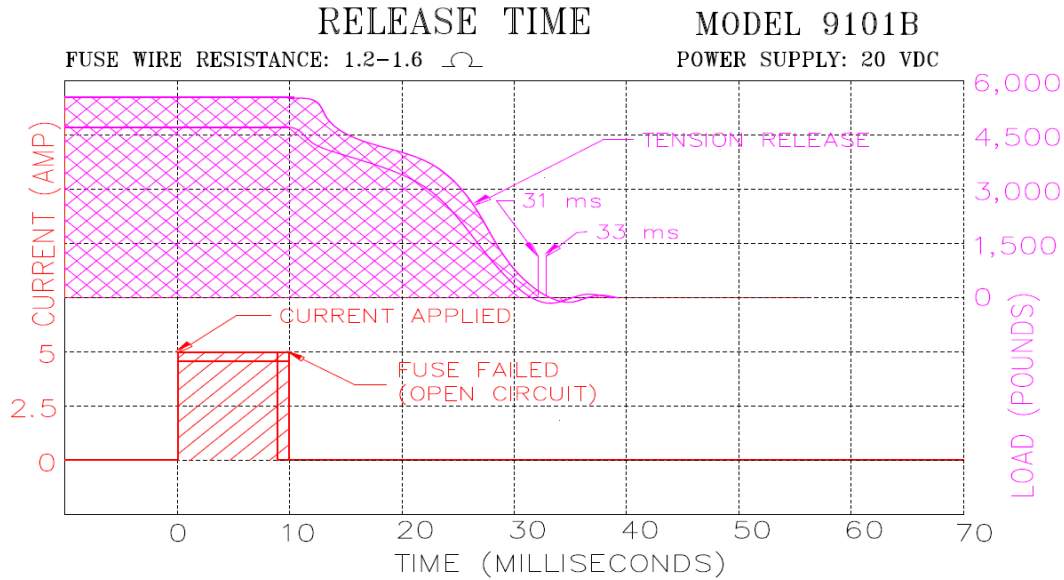
Figure 2.7.: NEA strain energy release [7]

The NEA is an off-the-shelf component with the following properties.

- Manufacturer: NEA Electronics, USA,
- Type: SSD-9100,
- Redundancy: single redundant fuse wire,
- Electrical interface: pyro-line, actuation current 3A at 20V,
- Qualified Temperature Rating: -135°C to +135°C,
- Mass: 70 g
- Release Load Rating: 6000 N

3. Drop Tower Campaign

This chapter gives an overview about the actual separation experiment with the boundary conditions, the test facility and the used test hardware.

3.1. MASCOT separation experiment

The test facility used was the drop tower at the CENTER OF APPLIED SPACE TECHNOLOGY AND MICROGRAVITY (ZARM) in Bremen. Microgravity is achieved by a free fall of a capsule in an evacuated drop shaft. The capsule which is used for the drops is shown in figure 3.1.
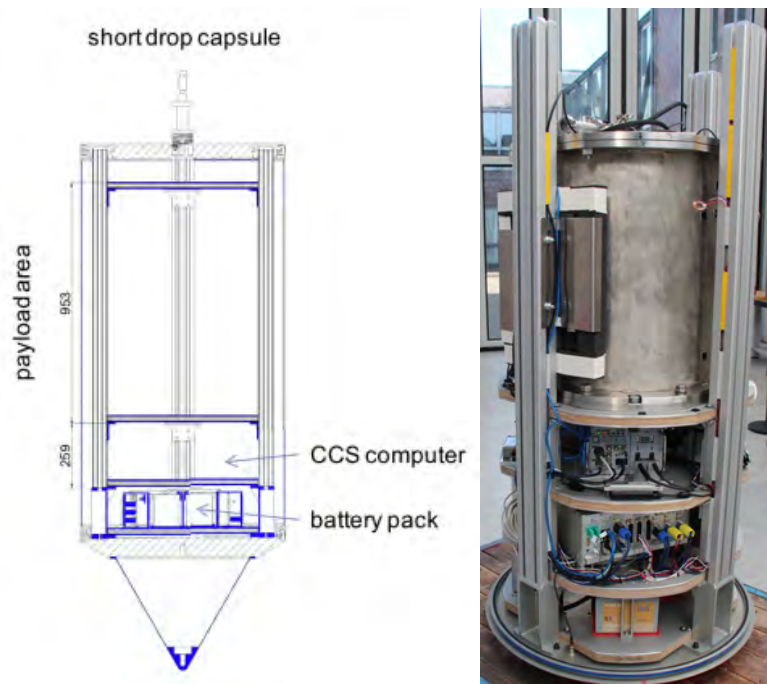

Figure 3.1.: Left: Schematic oft the drop capsule [9] Right: Drop tower capsule with the JAXA/DLR common camber

The capsule is dropped from a height of 110m and experiences approximately 4.7 s of near zero gravity. After the initial oscillations caused by the drop release have been damped down, residual accelerations of $10^{-7}\,g$ can be achieved. After the free fall the capsule is decelerated in a 13 m

container filled with fine polystyrene pellets. A maximum deceleration of 50 g for about 200 ms can act on the capsule. Figure 3.2 shows a typical plot of gravitational forces during deceleration inside the capsule.
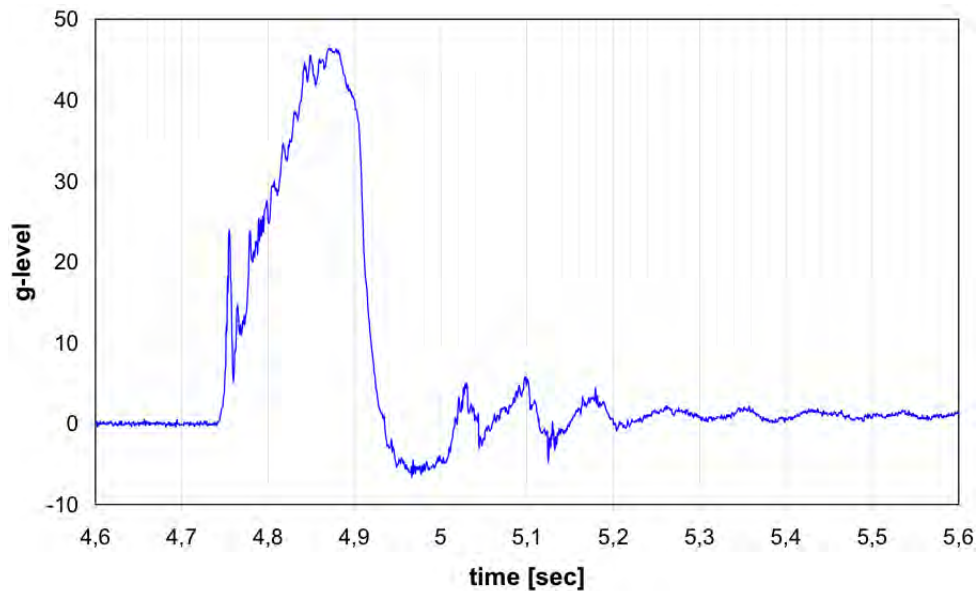
Figure 3.2.: Typical plot of gravitational forces during deceleration inside the capsule [9]

As it is not clear that the structure will survive the high deceleration forces and as the STM2.1 LM structure was at this time in another test campaign, the structure used for this drop test campaign was the STM1, which has already been used for the parabolic flight tests. The positions of the payload mass dummies included and listed in the following remained unchanged during the drop tests (figure 3.3).
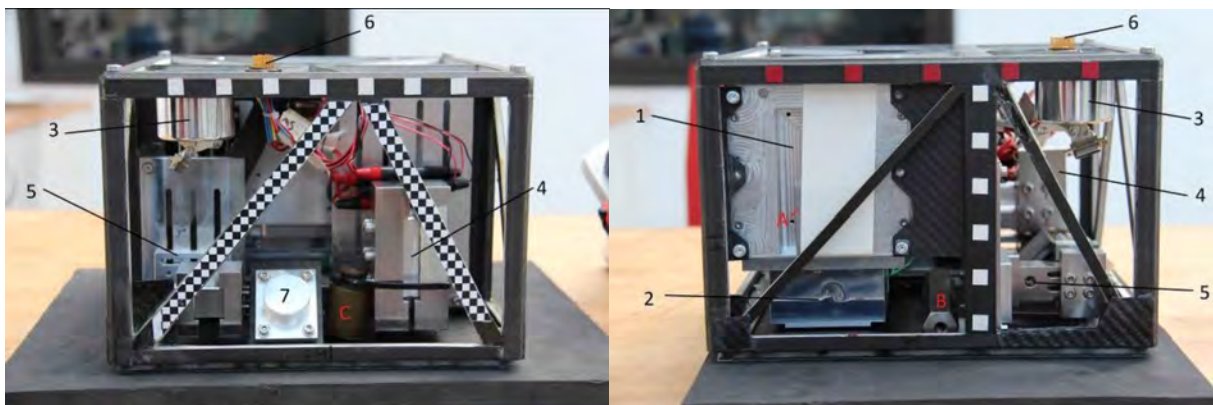
Figure 3.3.: MASCOT STM1 LM structure equipped with payloads mass dummies

1. E-Box, STM1

2. Primary battery, MD

3. Magnetometer (MAG), MD

4. Wide angle camera (CAM), MD

5. Microscope (MicrOmega), MD

6. Umbilical connector, EM

7. Radiometer (MARA), MD

In addition to the included subsystem mass dummies, the module is equipped with the following additional masses to trim the CoM, giving also the possibility to shift the CoM during drops. The used masses are shown below in figure 3.4 and their positions are exemplary seen in figure 3.3 above.
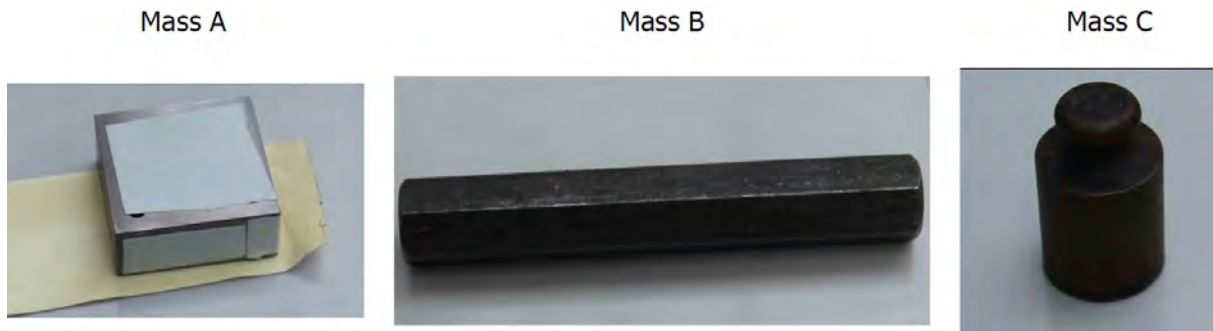
Figure 3.4.: Additional masses placed inside the LM to trim the CoM

The center of gravity (CoG) was measured and stated in table 3.1 with respect from the outer edges as defined in figure 3.5. The stated mass includes the whole configuration except the bolt from the NEA ($m_{Bolt} = 27\,$g, including nut and washer), which remains at the MESS after separation.
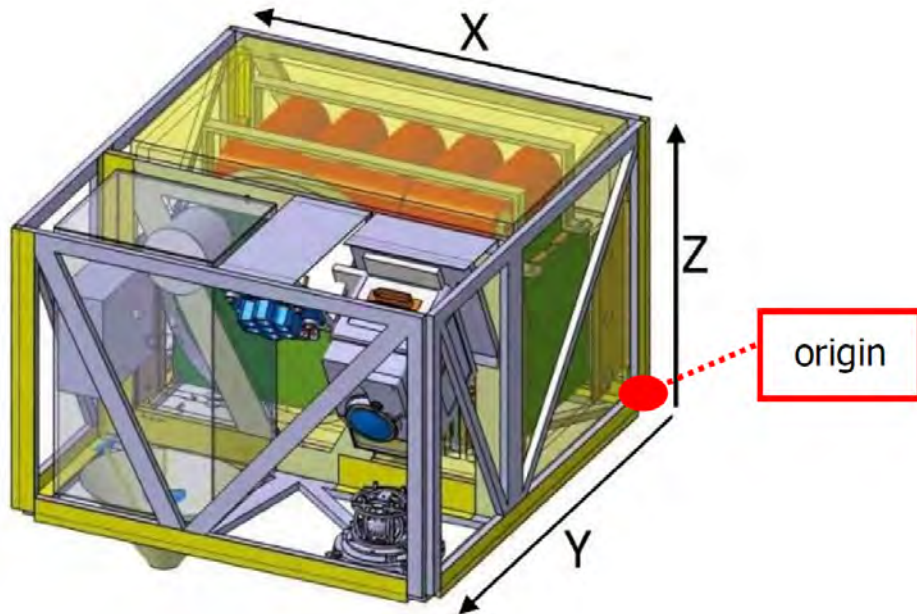
Figure 3.5.: CAD-model with a schematic of CoM origin and the regarding coordinate system

The resistance of the NEA coils is also measured before integration with a multimeter (FLUNKE 179) and given also in table 3.1.

Another element which was changed during drops was the MUSC (Mascot Umbilical and Science Connector). Here, the two parameters considered were the number of pins and the amount of washers below the interface screws. The latter was used to adjust the compression distance of the pins and hence the push energy. An example with one washer and twelve pins is shown in figure 3.6.
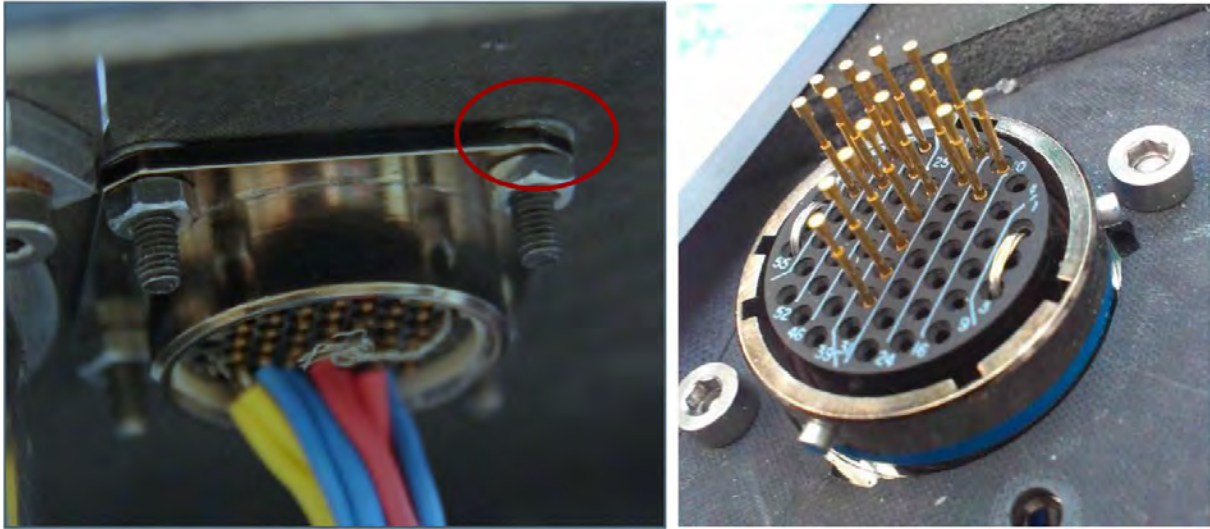
Figure 3.6.: MUSC (LM side) showing displacement washers (left) and the pogo pins (right).

Drop No. Date	CoM [mm]	Mass [g]	Umbilical configura- tion	NEA resistance [Ω]	Preload [N]	Comments/ Notes
accuracy	± 1 mm	± 1 g	-	± 0.1 Ω	± 5 N	-
1 26.03.2013	X: 147 Y: 132 Z: 114	7993	49 pins 2 washers	rd...rd: 1.5 bk...bk: 1.7	Initial:205 Final:188	Separation failed due to a cant of the main bolt
2 27.03.2013	X: 147 Y: 133 Z: 119	7981	12 pins 4 washers	rd...rd: 1.4 bk...bk: 1.3	Initial:212 Final:203	No IMU data (trigger failure)
3 28.03.2013	X: 139 Y: 147 Z: 114	7991	12 pins 4 washers	rd...rd: 1.5 bk...bk: 1.5	Initial:220 Final:194	No IMU data (trigger failure)
4 02.04.2013	X: 147 Y: 132 Z: 114	7993	49 pins 2 washers	rd...rd: 1.3 bk...bk: 1.5	Initial:228 Final:205	Camera (+X) and (+Y) failure
5 02.04.2013	X: 147 Y: 132 Z: 114	7988	49 pins 2 washers	rd...rd: 1.7 bk...bk: 1.7	Initial:235 Final:225	Camera (-Z) failure

Table 3.1.: Configuration of Mascot at the single drops

3.2. DTC test hardware and equipment

3.2.1. DLR/JAXA Common Chamber

Inside the main capsule frame were used the common vacuum chamber provided by JAXA as an interface and controlled environment for the actual separation experiment. In defiance of the name, we used however no vacuum inside the chamber as the effect of air drag by the ambient pressure is negligible for such a comparable big free floating object and the low separation velocity of approximated $0.05\,\frac{m}{s}$. The chamber is seen in Figure 3.7 as a CAD-model which was designed based on measured values. It is manufactured from stainless steel and its inner dimensions are $0.5\,m$ in diameter and $0.6\,m$ in height. The mass is about $130\,kg$.
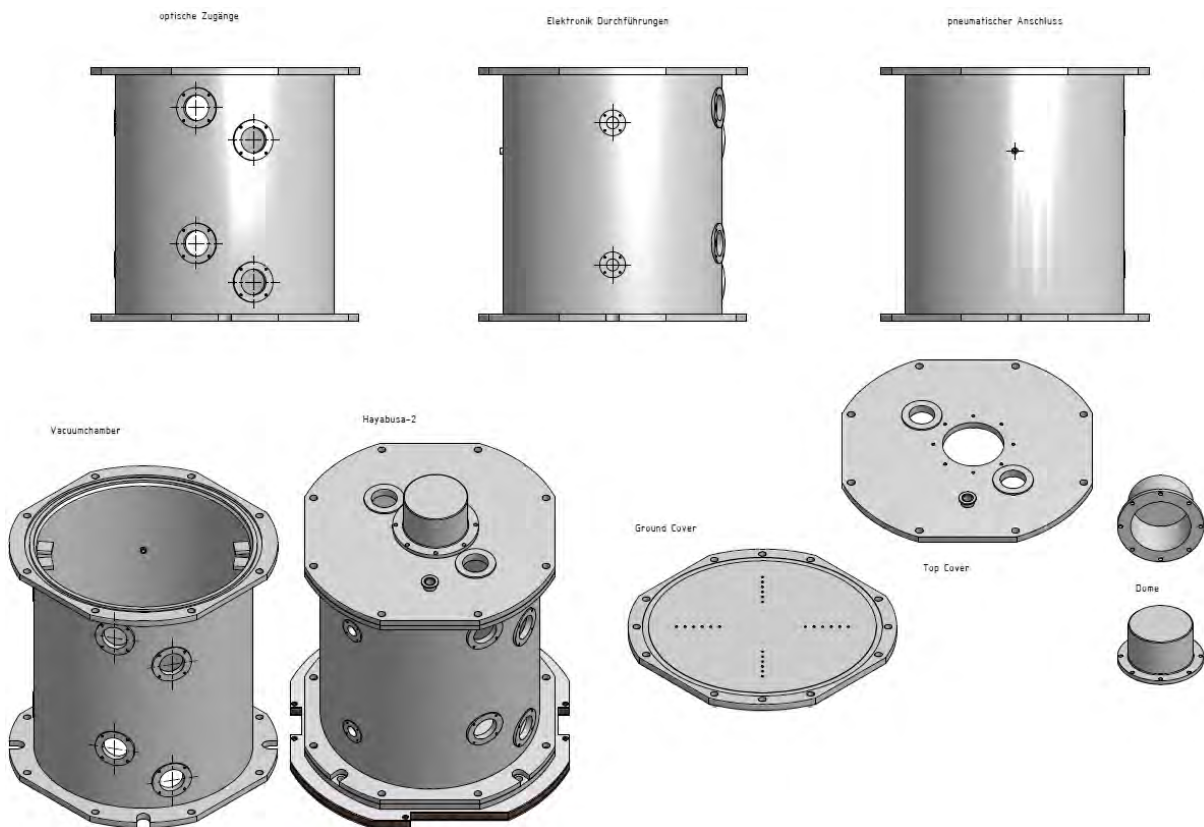
Figure 3.7.: CAD-model of the JAXA/DLR common camber

At the bottom of the chamber is a cushion placed in order to prevent a damage of the structure. The cushion is filled withe a foam material. The top and the bottom of the cushion were covered with VELCRO® to avoid a rebound of the landing module back into the MESS after deceleration at the end of the micro gravity phase. In the middle of the cushion is a round cutout with 45° chamber to not minimize the field of

The Cushion is shown in Figure 2.15.
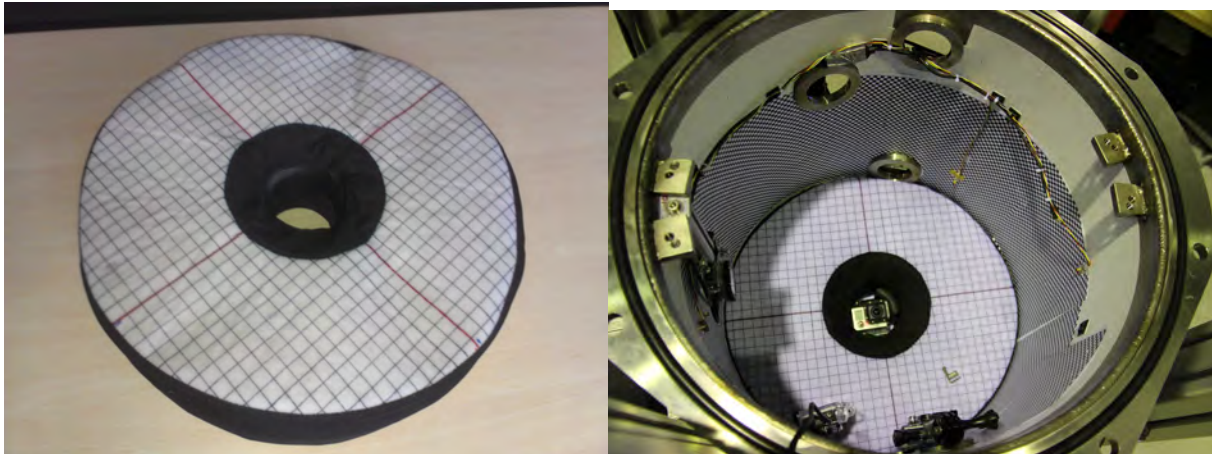
Figure 3.8.: MASCOT deceleration cushion

There is a interface designed to place MASCOT inside the common chamber.It is responsible for a safe and ridged mounting and a vertical separation direction of the LM straight downwards. The interface is shown in figure 3.9.
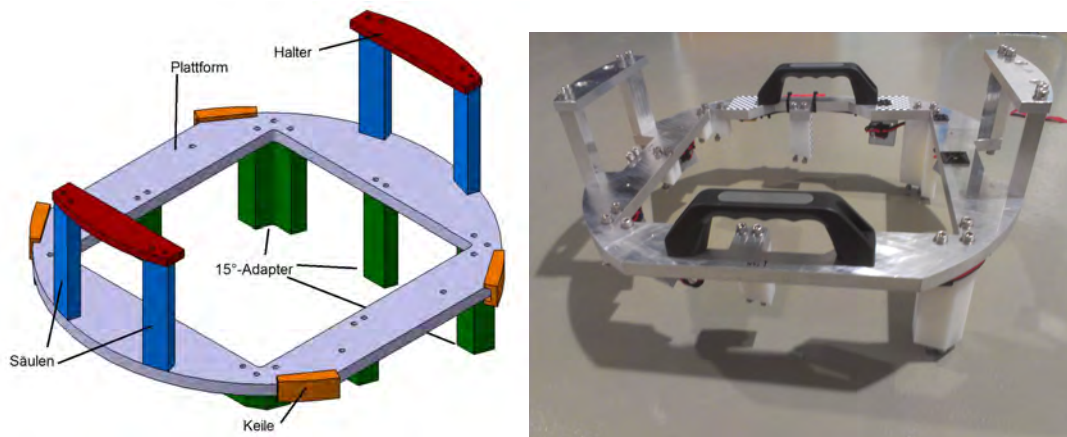
Figure 3.9.: MASCOT to common chamber interface

For a better overview of the test assembly is in figure 3.10 a CAD model of the common chamber equipped with the interface and the deceleration cushion.
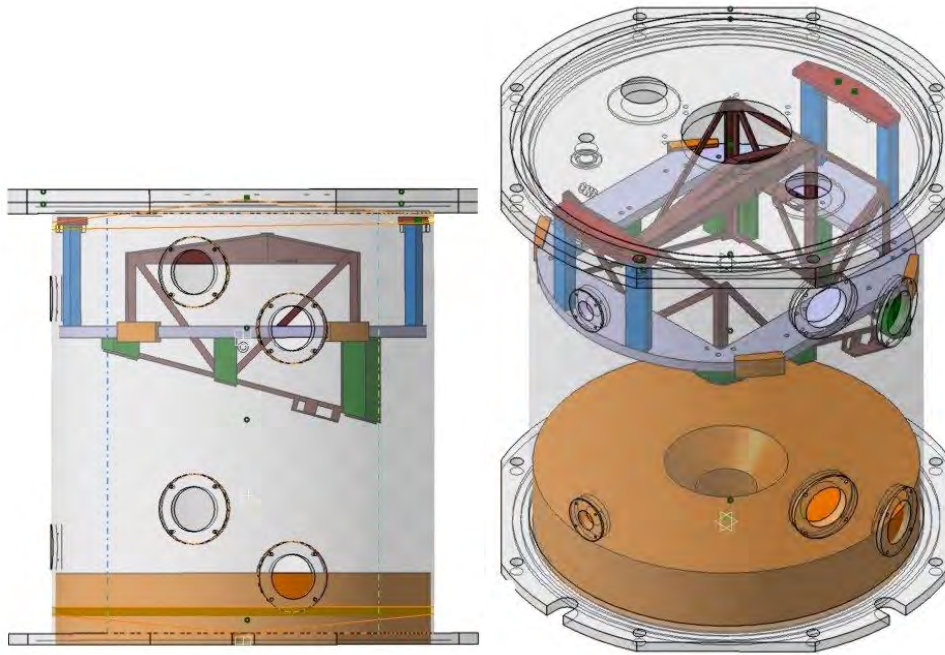
Figure 3.10.: Overview of the common chamber with the interface and the deceleration cushion

3.2.2. Inertial Measurement Unit

To measure the occurred accelerations which act on the MASCOT LM during separation, a inertial measurement unit (IMU) is installed inside the LM as close as possible to the CoM. By integrating this acceleration data the velocity and the trajectory of the LM can generated. The IMU that is used is a stand-alone data logger with a battery and a Micro-SD-Card as a memory medium inside, so no wire connection is required.

Figure 3.11.: x-io Technologies inertial measurement unit [10]

The IMU is an off-the-shelf component with the following properties [10].

- Manufacturer: x-io Technologies Limited, UK
- On-board sensors

    - Triple axis 16-bit gyroscope – Selectable range up to ±2000 °/s

    - Triple axis 12-bit accelerometer – Selectable range up to ±8 g

    - Triple axis 12-bit magnetometer – Selectable range up to ±8.1 G

    - 12-bit battery voltage level

    - Factory calibrated

    - Temperature compensated (gyroscope only)

    - Selectable data rates up to 512 Hz

- Dimensions: $33 \times 42 \times 10$ mm ($57 \times 38 \times 21$ mm with plastic housing and battery)
- Weight: 12 g (49 g with plastic housing and battery)

3.2.3. Cameras

The used camera systems are used not only for visual observation of MASCOT during the test but also video analysis and image tracking. For this purpose the module was supplied by hand-made sticky markers put straight on the main structure and payloads. The positioning of the markers was chosen in the way that they would be first placed within the focus of camera and second would be as close as possible to expected location of CoM plane. One marker is a 10x10 mm square tape. This size and shape allow to clearly recognize it in the video image and to use as a reference point in the video analysis and modeling tool TRACKER.
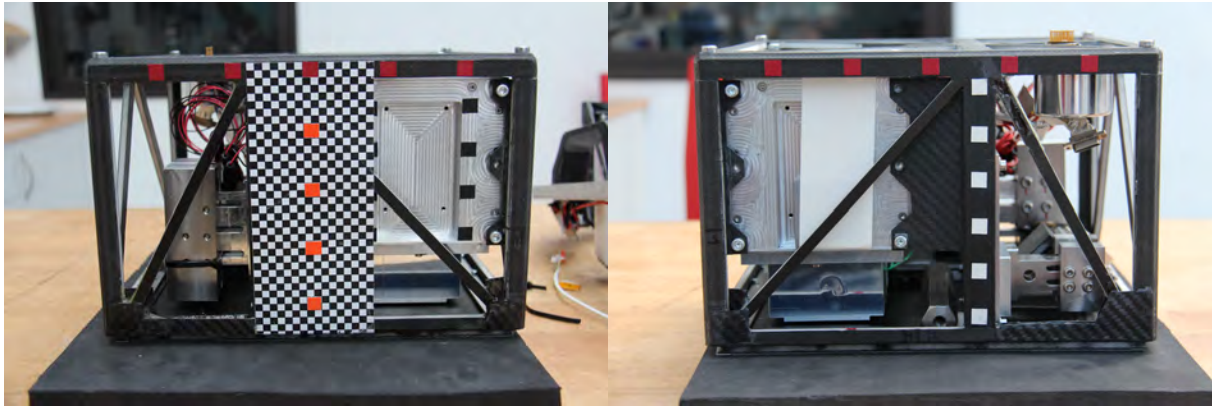
Figure 3.12.: MASCOT LM with optical markers. Left: pos. X, Right: neg. X
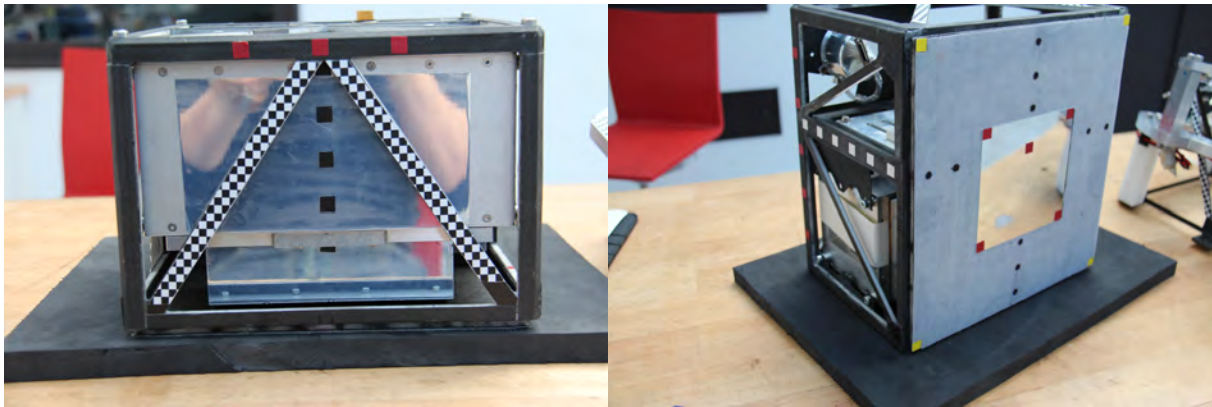
Figure 3.13.: MASCOT LM with the optical markers. Left: pos. Y, Right: neg. X respectively main radiator

Another important part of placing the markers is a reference scale. For this, the markers were placed in a chess pattern put both on the inner surface of the chamber and on some struts of the structure, that can be seen in figure 3.12 and 3.13.

GoPro Action Cameras

Due to a shortage of space inside the common chamber between the inner wall and the MASCOT module, small and robust action cameras are used. There are four GOPRO HERO3 cameras used foreseen to obtain maximum visual information about MASCOT´s behavior at the separation moment and further while free falling. These cameras were uniquely positioned in the test chamber so that MASCOT could be observed from three axes: along the X and Y positive direction and Z negative direction, respectively. Thus two cameras were set on one side of the chamber (+X axis) one above the other in order to see the separation process itself as well as

the module descending. The third camera (+Y axis) is oriented with respect to these cameras at the angle of 90° in horizontal plane and the last one was placed at the bottom of the chamber in the center of the deceleration cushion looking upwards to the main radiator figure .
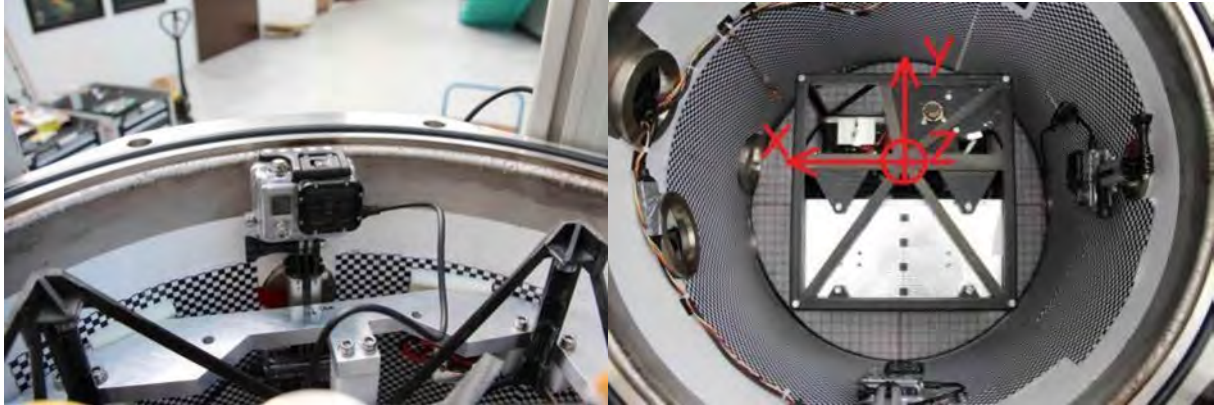
Figure 3.14.: Position of the GoPro cameras inside the common chamber with respect to MAS-COT´s coordinate system

All cameras had the same settings mode with a video resolution of 960 p at 30 fps and a field of view of 170°.

Photron Factcam MC2^{TM}

The used digital high-speed video system is provided by ZARM and belongs to the optional capsule set up. This system is a Photron Factcam MC2^{TM}, consists of a processor and two camera heads like seen in figure 3.15. It is based on light sensitive CMOS imaging sensors.

Figure 3.15.: Photron Fastcam MC2 with dual camera head [9]

The camere heads are mounted on the DLR/JAXA common chamber and can film the experiment through the holes on the camber side. By mirrors (figure) which are inclined in an angel of 45° it is possible to place the camera heads between the common chamber and the outer wall of the drop capsule. At the same time the focus distance can be extend to yield a sharp picture. This camera system is primary to film the initial moment of the separation with the upper head and the final moment of landing on the cushion with the lower head. By this data the separation velocity can later calculated.
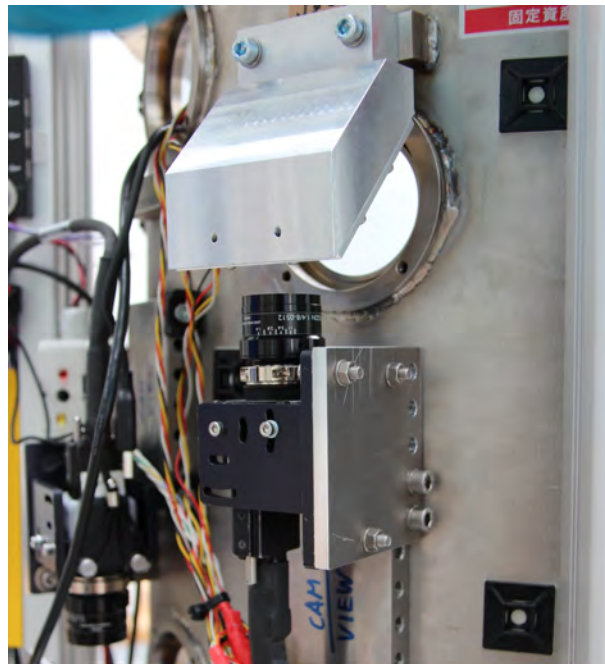
Figure 3.16.: Photron Fastcam MC2^{TM} camera head and a mirror mounted to the common chamber

The Photron Fastcam MC2^{TM} has the following properties .

- Two remote camera heads (35 mm x 35 mm x 35 mm; 90 g; without lens),
- 512 x 512 pixel resolution,
- 2000 f/s at full image resolution, for both camera heads and 4 s recording time,
- 1000 f/s at full image resolution, for both camera heads and 8 s recording time,
- up to 10.000 f/s with reduced image resolution (512 x 96 pixel),
- Global electronic shutter from 20 ms to 6 μs,
- Color (24 Bit) or monochrome (8 Bit),
- Cameras precisely synchronized to an external source,
- Lens mount: C-mount,
- Remote camera heads with 3 m cable for easy positioning at hardly accessible space,
- Processor unit (H: 195 mm x W: 159 mm x D: 130 mm; 5 kg),
- Live Video during recording, NTSC, PAL
- Ethernet camera control
- Start, End, Center and Manual Trigger Modes,
- Saved formats: JPEG, AVI, TIFF, BMP, RAW, RAWW, PNG, FTIF,

3.2.4. Ring Load Cell

Measurements of the preload shall be enabled through a miniature ring load cell, Model 8438-6010 from Burster shown in figure 3.17.
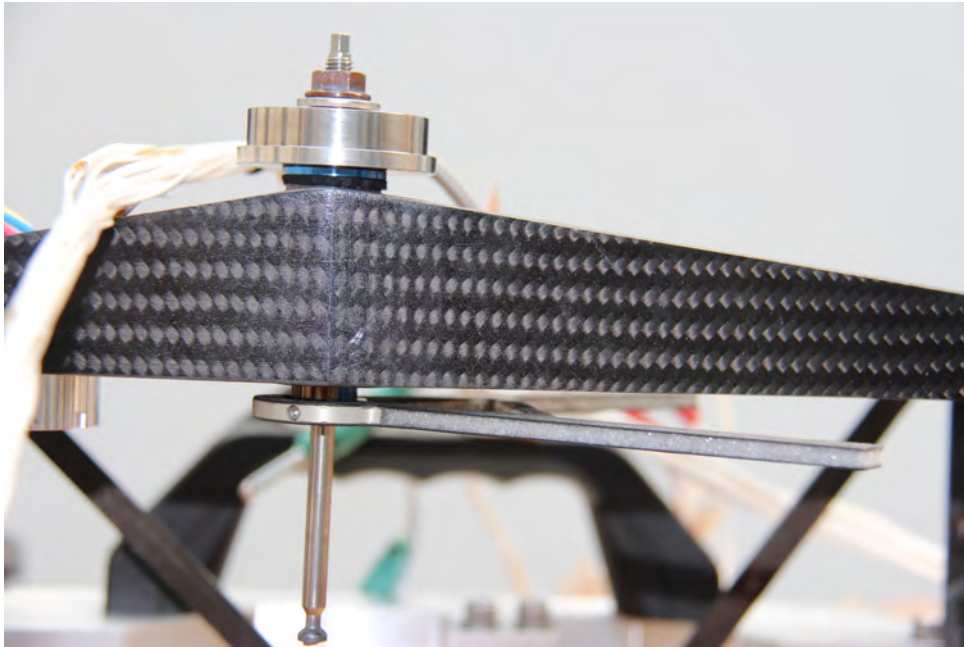
Figure 3.17.: Burster ring load cell 8438-6010

The measured tension and compression force has to be introduced axially and perpendicularly to the entire surface of the inner and outer rings of the sensor in opposite directions to obtain usable results. The sensor works with strain gauges which changes their electric resistance by strains, even by small ones. So the force sensor converts the acting force into an electrical output signal. This signal is processed by an amplifier, especially 9236-V300 from Burster seen in figure 3.18. The amplifier amplified the analog signal from mV to V. This signal is sent to the CCS, which converts the signal into a digital one and logs it in the date acquisition inside the CCS.
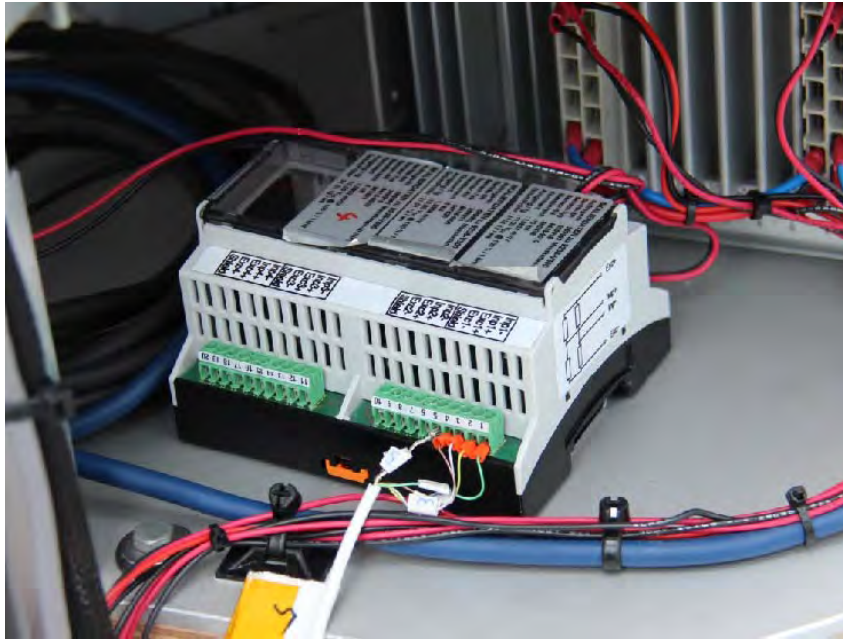
Figure 3.18.: Amplifier used for the ring load cell signal

By calibration with the aid of a second already calibrated force sensor the ratio between voltage and force is determined. The following equation 3.1 describes the relation.

$$\frac{U}{F} = C = 0,00122\frac{V}{N} \tag{3.1}$$

With U is here the output voltage from the amplifier, F is the force given by already calibrated sensor and C is the yielded coefficient for conversion. With the aid of this equation the diagram in figure 3.19 is generated.
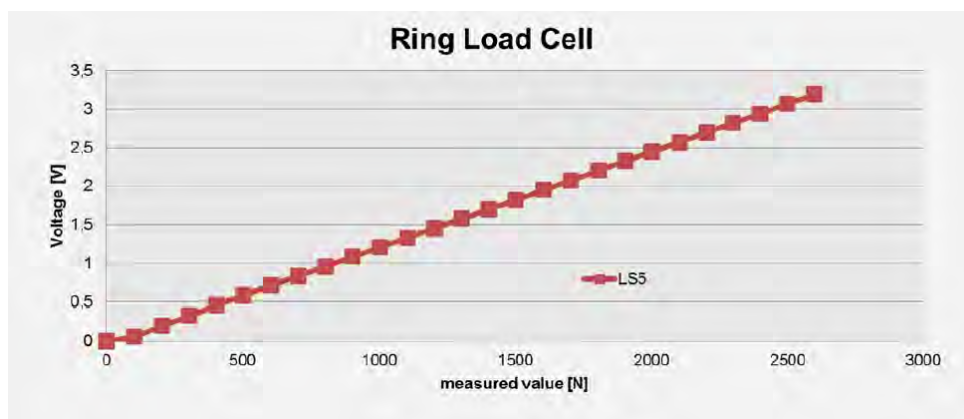
Figure 3.19.: Diagram of measured voltage and corresponding force

Four wire measurement techniques is used to prevent measurement errors By this, one pair of wires carries the excitation current and the other pair connects to the voltage measuring instrument, which, ideally draws no current. Thus any voltage drop on the wires carrying the excitation current is not measured and does not contribute an error.

The data sheet of the ring load cell can be found in appendix.

4. Test analysis

4.1. IMU data

The x-IMU stores all logged data in a binary file (.BIN). This file can converted with the x-IMU-GUI in several Comma-separated values file (.csv). which contains the data of the single sensors of the IMU. After working off the data, a transformation from regarding to the LM fixed coordinate system to a MESS fixed coordinate system and integration the data were analyzed. The so occurred separation velocity and trajectory were significant different to the data yield by optical measurements. This leads to the case that for the analysis just the data occurred from the cameras were usable.

4.2. Video data

The video analysis concentrates on getting a quantifiable picture of the MASCOT descend motion after the separation moment. This task is performed by means of video analysis. During image processing the following features were used.

- manual and automated object tracking with position, velocity and acceleration overlays,
- applying video filters, including brightness/contrast, ghost trails, and deinterlacing filters,
- correction for radial distortion associated with fisheye lenses,
- controlling video properties such as video dimensions, path, frame rate, frame count and more,

First the radial distortion in the video is corrected as the image must be close to the real properties of the object like seen in figure 4.1.
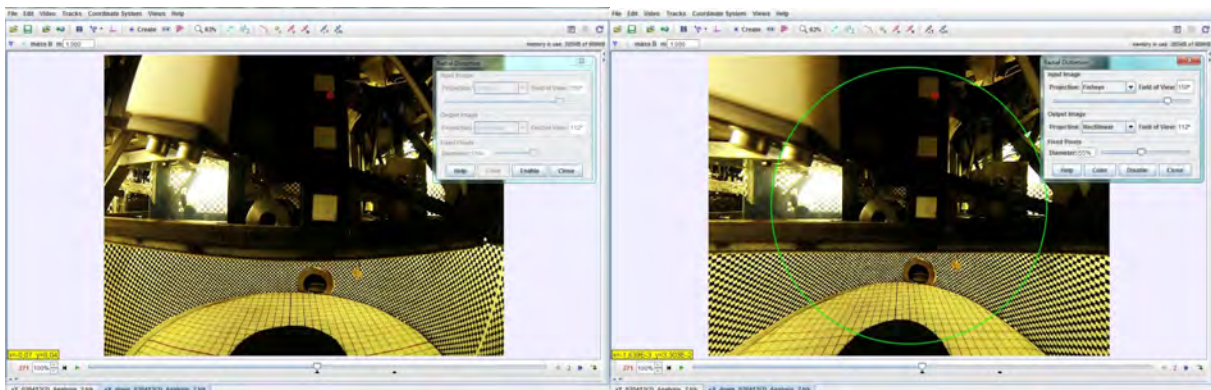
Figure 4.1.: Before and after distortion correction

The frames to analyze were identified, which are regularly the frames containing the movement from start to end, calibrated the scale to the known dimension of the markers and set the origin of the reference to the outer edge of the Main Radiator and MASCOT´s middle wall (Figure 4.2).
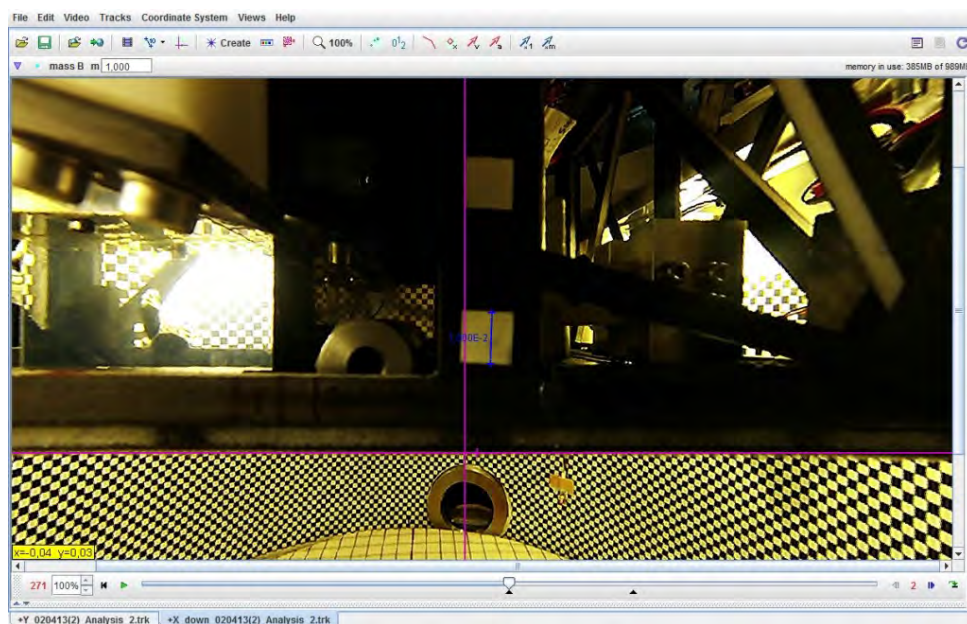
Figure 4.2.: Calibration and definition of the origin
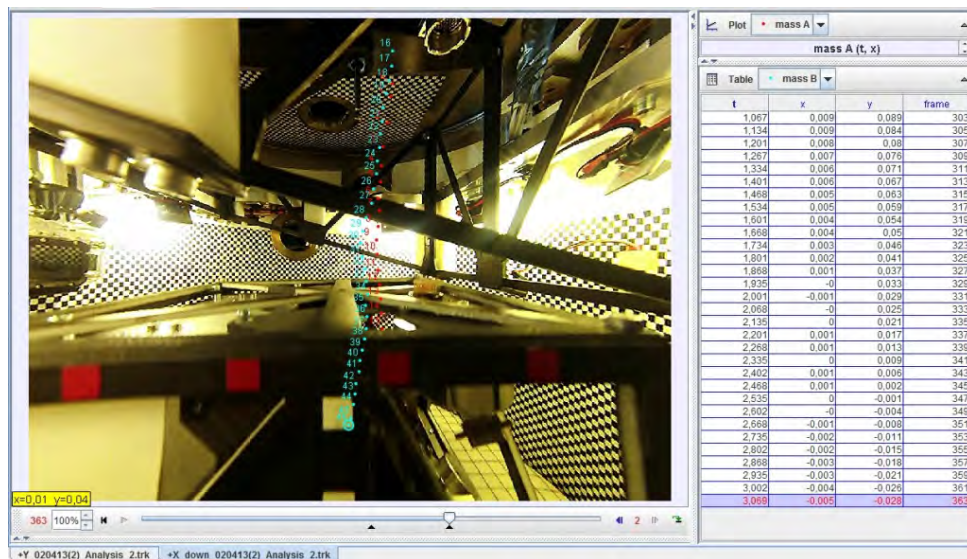
Figure 4.3.: Tracking process

By tracking a specific marker was a range of coordinates obtained corresponding to each position in time. Combining and correlating them with those from other orthogonal video angle a coordinate matrix that contains X, Y, Z components was established determining the movement of an imaginary point located at the virtual intersection of the traced markers (Figure4.3). The graphical visualization of the path was then fulfilled in MATLAB. The trajectories of drop no.2, 3 and 5 are shown in figures 4.4, 4.5 and 4.6.
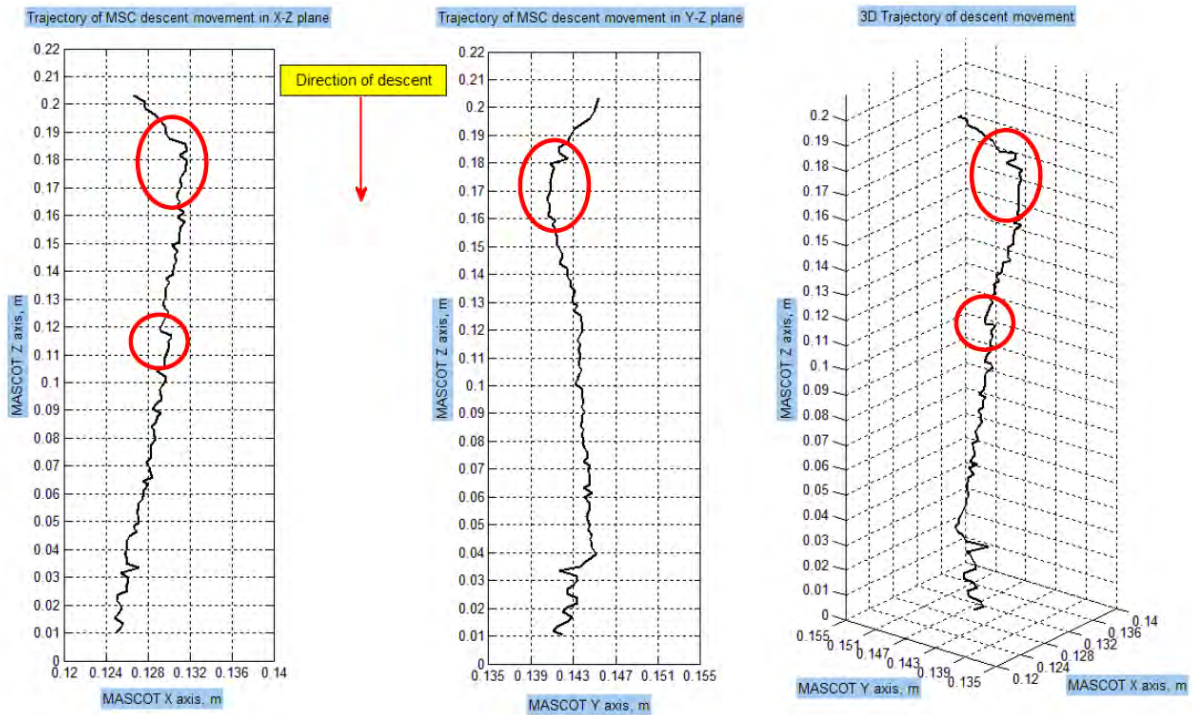
Figure 4.4.: Trajectory drop no.2
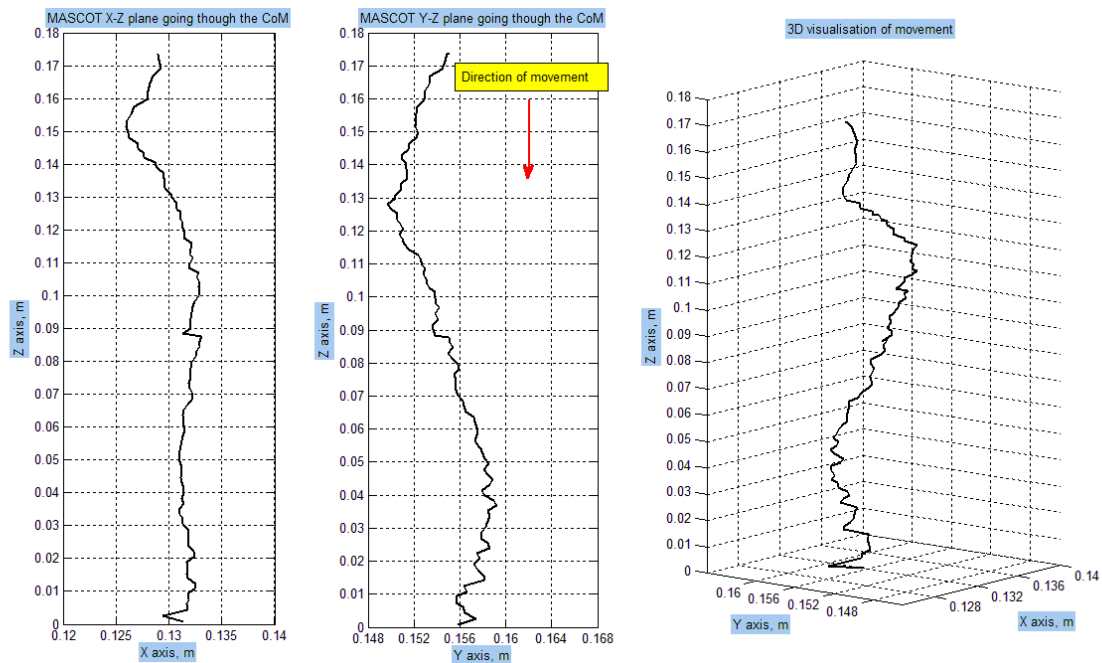
Figure 4.5.: Trajectory drop no.3
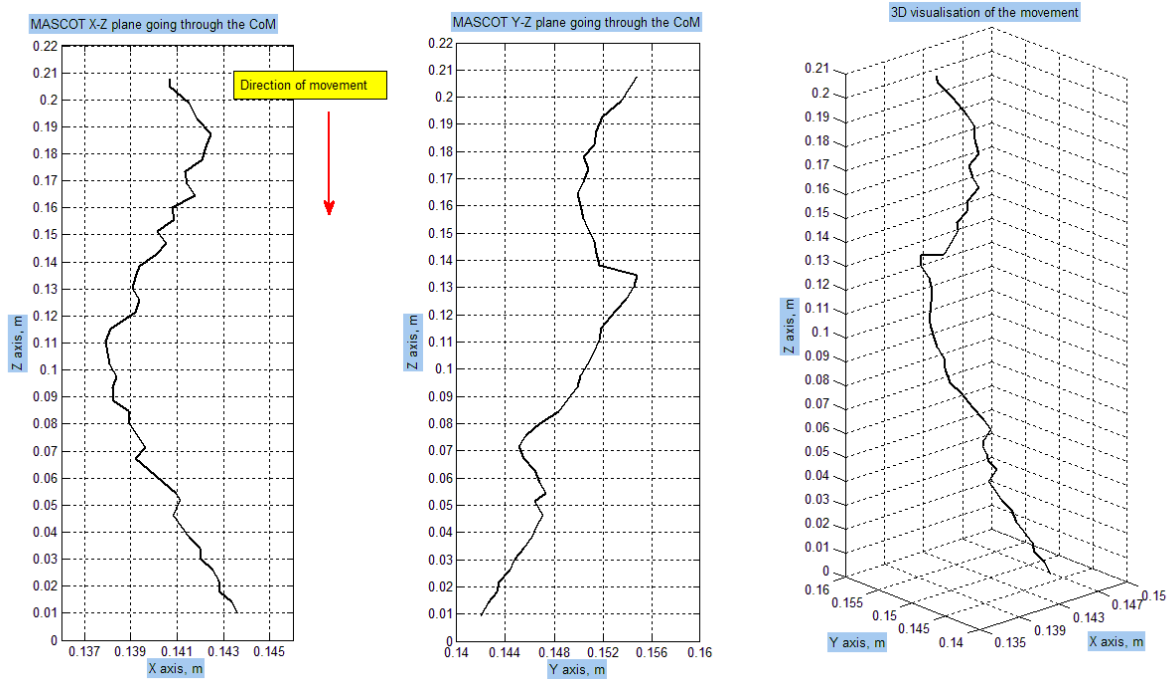
Figure 4.6.: Trajectory drop no.5

In a similar process, for determining the eject velocity of the module, the start and landing video sequence was analyzed of the images taken by the PHOTRON FACTCAM MC2 high speed cameras with a resolution properties 512p and 250fps.

The results for drop no.2 and 3 are given in table 4.1 and the results for drop no.4 and 5 are given in table 4.2.

Drop #2

0,928 seconds after separation:

Nr. of frames	time, s	path, m	V, m/s	V, cm/s
232	0,93	0,05	0,054	5,4

1,6 seconds after separation:

Nr. of frames	time, s	path, m	V, m/s	V, cm/s
168	0,67	0,034	0,051	5,1

2,528 seconds after separation:

Nr. of frames	time, s	path, m	V, m/s	V, cm/s
232	0,93	0,047	0,05	5,0

Landing:

Nr. of frames	time, s	path, m	V, m/s	V, cm/s
300	1,2	0,058	0,048	4,8

Drop #3

0,888 seconds after separation:

Nr. of frames	time, s	path, m	v, m/s	v, cm/s
222	0,89	0,0496	0,0558	5,58

1,451 seconds after separation:

Nr. of frames	time, s	path, m	v, m/s	v, cm/s
134	0,54	0,0296	0,0553	5,53

2,627 seconds after separation:

Nr. of frames	time, s	path, m	v, m/s	v, cm/s
294	1,18	0,054	0,0459	4,59

Landing:

Nr. of frames	time, s	path, m	v, m/s	v, cm/s
320	1,28	0,058	0,0455	4,55

Table 4.1.: Generated results for drop no.2 and 3

Drop #4

0,752 seconds after separation:

Nr. of frames	t, s	path, m	V, m/s	V, cm/s
188	0,75	0,049	0,065	6,48

1,296 seconds after separation:

Nr. of frames	t, s	path, m	V, m/s	V, cm/s
136	0,54	0,038	0,07	7,03

1,936 seconds after separation:

Nr. of frames	t, s	path, m	V, m/s	V, cm/s
160,00	0,64	0,042	0,066	6,59

Landing:

Nr. of frames	t, s	path, m	V, m/s	V, cm/s
188	0,75	0,05	0,068	6,76

Drop #5

0,68 seconds after separation:

Nr. of frames	time, s	path, m	v, m/s	v, cm/s
170	0,68	0,045	0,0654	6,54

1,12 seconds after separation:

Nr. of frames	time, s	path, m	v, m/s	v, cm/s
110	0,44	0,024	0,0553	5,53

1,92 seconds after separation:

Nr. of frames	time, s	path, m	v, m/s	v, cm/s
200	0,8	0,045	0,0556	5,56

Landing:

Nr. of frames	time, s	path, m	v, m/s	v, cm/s
200	0,8	0,053	0,066	6,61

Table 4.2.: Generated results for drop no.4 and 5

4.3. NEA strain energy release

The plot in figure 2.7 which shows the strain energy release regarding to the actuation signal in both coils of the NEA. This plot is given by NEA ELECTRONICS. With a delay of about 12 ms the preload starts to decline and achieves a zero value after 31 ms.
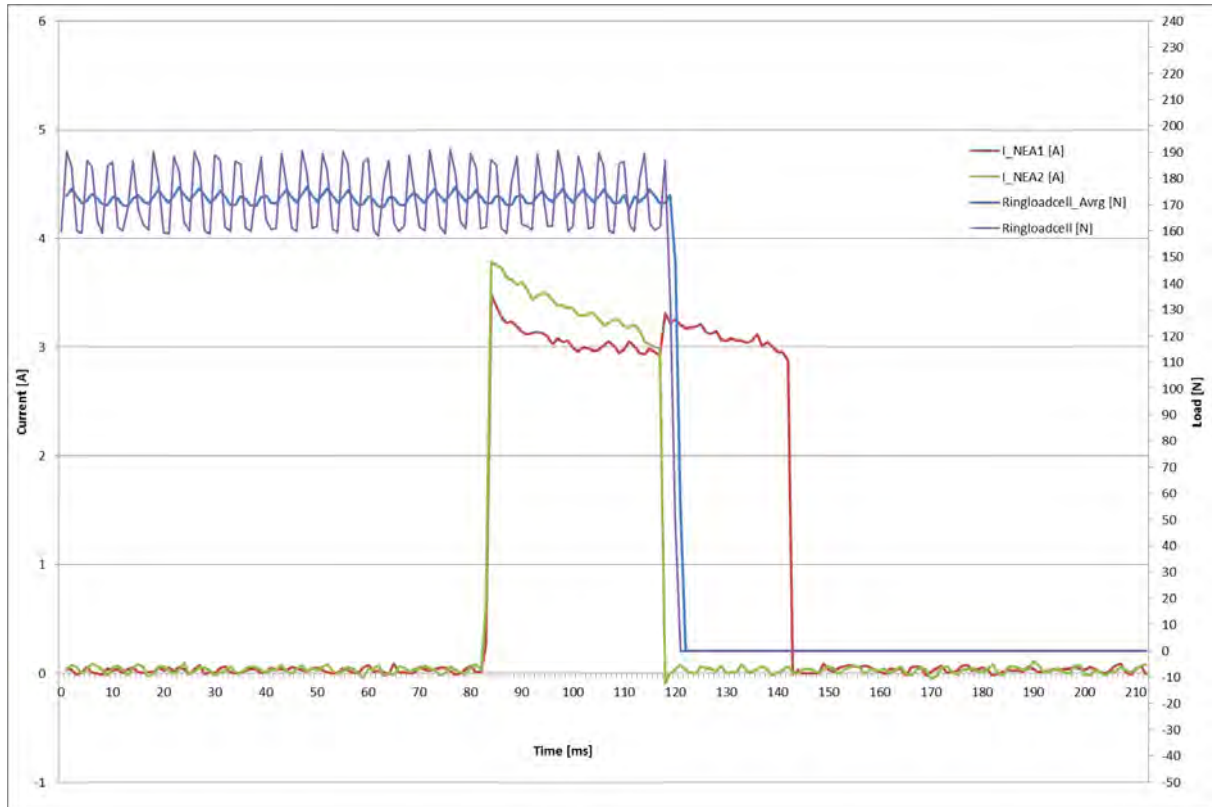

Figure 4.7.: NEA strain energy release drop no.4

The plot in figure 4.7 shows the measured data at the fourth drop. The decline of the preload value starts here with a delay of 35 ms and achieves a zero value after 40 ms. The rapid decline of the preload graph is based on the awareness of the spring inside the separation mechanism assembly.

5. Conclusion

5.1. Analysis results

The graphs in section 4.2 show the separation of the LM out of its support structure. It can be seen that the overall movement is along the vertical axis, which is the nominal separation direction. The LM moves a distance that is a bit higher than 20 cm until it touches the deceleration cushion. This ensures that the LM quits the MESS frame .

As described in section 4.2, the trajectory plotted in the graphs is a combined track from three different viewing angles joining in a single imaginary point located at the virtual intersection of the traced markers.

The small corrugations on the curves are caused by a manual error that occurs due to inaccuracy of tracking symbol positioning during work off with the tracking software. The visible deviations to either sides are approximately in the order of magnitude of a few millimeters. These deviations leads to make contact with the frame of the support structure. The positions where the LM has a collision wit the MESS are marked with red circles. After the rebound it has a another collision or it quits the MESS frame entirely. On the images it also can be seen that the LM, when it clears the MESS, tends to rotate slightly around its x-axis. This is caused by the contacts it makes with the MESS which cannot be predicted and which happens arbitrary.

Specifically the last contact determines the final direction of motion, as there is no guidance after leaving the MESS. The resulting angle of the separation direction with respect to the $+15°$ from HY2-Y-Panel of the main S/C varies therefore significantly from -1° in drop no.2, -12.8° in drop no.3 and -8.2° in drop no.5. Hence, drops no.3 and no.5 violate the $\pm5°$ deployment inaccuracy stated. The velocity of the LM is shown in table 4.1 and table 4.2. As stated above, the last contact with the MESS determines the final direction of motion as well as the final separation velocity. Therefore, the LM velocity after it clearance of the MESS frame is considered. Drops no.2 and no.3 show similar eject velocities as well as drops no.4 and no.5. This is caused by the configuration changes listed in table 3.1. Subsequent to the first drop, the amount of pins of the umbilical connector was reduced. In order to minimize the additional push as a result of the compressed springs inside the pogo pins to a minimum. The only using those pins required to transmit the activation current. This was changed for drops no.4 and no.5. The velocity is in average of 4.7 $\frac{cm}{s}$ with minimized connector impact and 6.7 $\frac{cm}{s}$ with the fully equipped connector.

5.2. Discussion

The systematic introduction of a moment around the x-axis was overcome by a completely iterated and newly designed v-shaped push-off plate. The separation failure occurred in drop no.1 was due to an inaccurate integration of the NEA. This led to a misalignment with the separation shaft. The position of the NEA inside the LM structure caused a non coincidence of the bore holes, which is shown in figure 5.1. Apart from that it could be verified that if integrated correctly, separation of the used configuration was successful 4 out of 4 times. Therefore, integration of the MASCOT SepM should be given a high priority, performed with an integration procedure and checked via quality management and the design should be put under close configuration control. A lessons learned document lists these suggestions to avoid inter alia a incorrect integration. These changes should be taken into account for the QM/FM design. This document is appended.
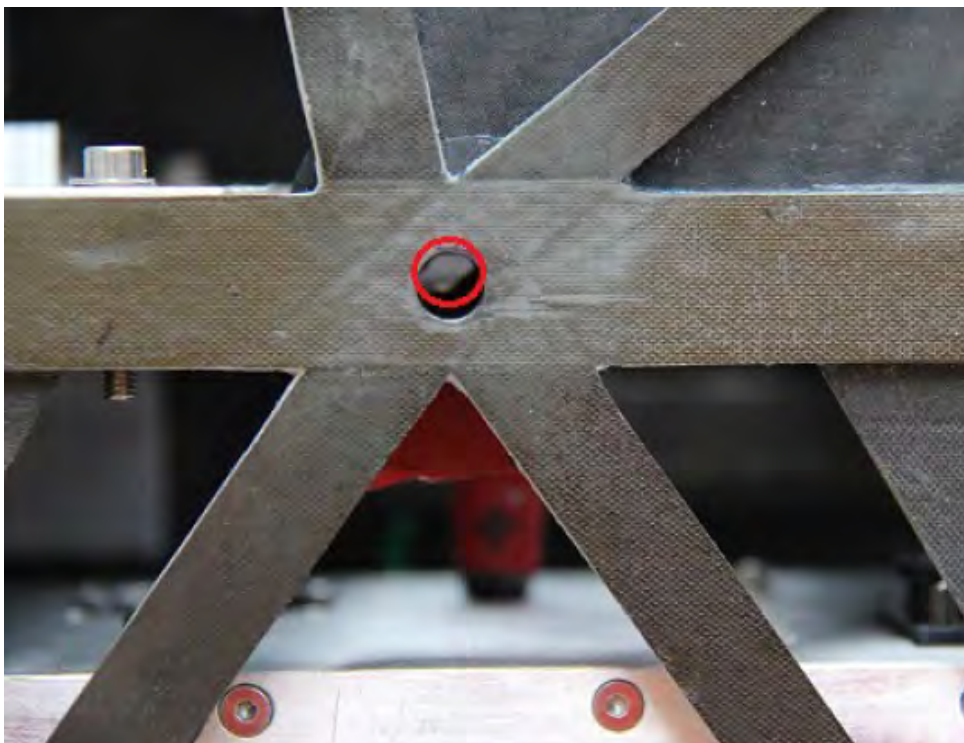

Figure 5.1.: Close-up on the separation shaft and indication of the NEA misalignment

5.2.1. Thermal Aspects

The performed separation test only took into account the functionality of the system in microgravity condition and not in an appropriated thermal environment. As material properties and behavior can change in very high or very low temperatures the functionality of the system should also be verified in thermal vacuum conditions. Thermal influences have an effect on inter alia

the properties of the separation spring this will change the kinetic energy which is put into the system.

"For one-shot systems it is all too easy to accept a few deployments in the laboratory as verification and then be mightily surprised when it fails to deploy in space because of temperature differentials" [P. Fortescue, Spacecraft Systems Engineering, Third Edition, 527]

5.2.2. Separation Trajectory

The test campaign showed that the LM, when it clears the MESS, tends to rotate very slightly around the x-axis. This is most apparent during the drops no.3 and no.5. This is not due to the push-off process itself, but again due to the contacts it makes with the MESS. These contacts cannot be predicted and happen arbitrary. Specifically the last contact determines the terminal vector change and the final direction of motion. The resulting separation angle with respect to the +15° from −Y panel of the main spacecraft (Figure 1.10) varies therefore significantly from -1° in drop no.2, -12.8° in drop no.3 and -8.2° in drop no.5. Hence, drops no.3 and no.5 violate the ±5° deployment inaccuracy. The nature of the unlock characteristics of the NEA, the release of the residual preload stored elastically in the MESS frame, the influence of the umbilical connector and the push-off process should be therefore investigated in more detail via numerical analysis as well as stand-alone laboratory tests of the push-off mechanism. These results should be incorporated in the QM/FM design and tested again for qualification in microgravity conditions.

5.2.3. Separation Velocity

The last contact with the MESS frame determines the final direction of motion as well as the final separation velocity. Drops no.2 and no.3 show similar eject velocities as well as drops no.4 and no.5. This was due to the configuration change with the umbilical connector. During the first drops, the amount of pins in the umbilical connector was reduced in order to minimize influence of the umbilical on the separation.. This was changed for drops no.4 and no.5. The velocity significantly increased by 30 % from an average of 4.7 $\frac{cm}{s}$ (drop 2 and 3) to 6.7 $\frac{cm}{s}$ (drop 4 and 5). It becomes apparent that the umbilical connector with its pogo pins has an significant impact of the eject velocity. The used pogo pins have a compression distance of 2.4 mm and a resulting spring force of 0.3 N. These small springs work in parallel so the effective spring force with a full set of 50 pins will add-up to 15N ($k_{eff} = 6.25 \frac{N}{mm}$). For comparison, the used separation spring has a spring constant of 0.27 $\frac{N}{mm}$ and a resulting spring force of approximately 12 N. As the force vector of the connector does not go through the CoM, the main push is still given by the push-off plate. Nevertheless, the connector introduces a significant force which increases the eject velocity. It also induces a moment around the x and the y-axis caused by its position. The impact of the connector should be investigated in more detail.
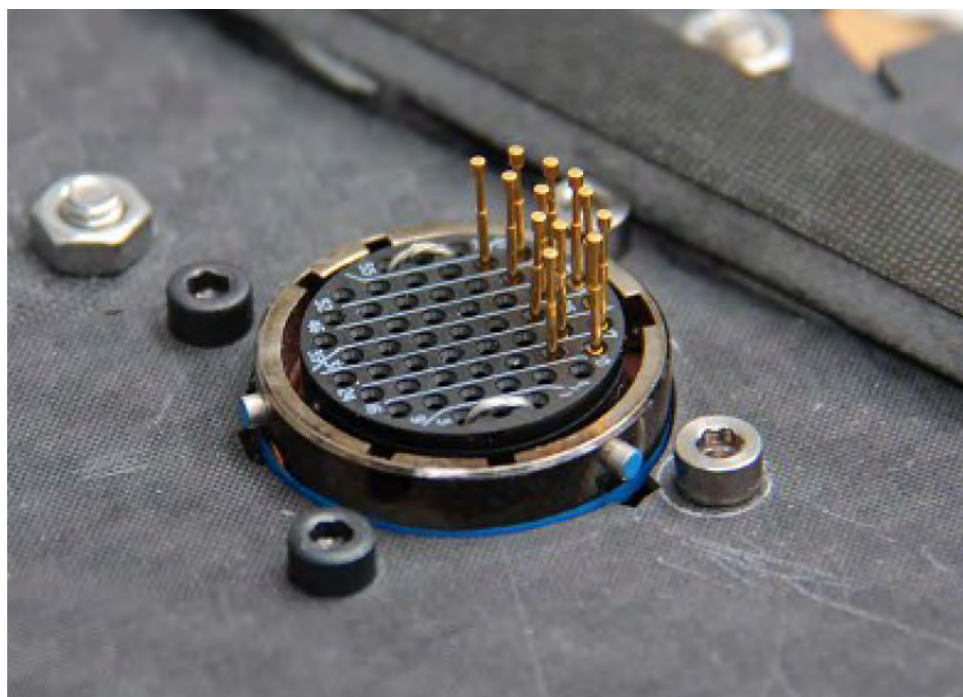
Figure 5.2.: MUSC equipped with 12 pins (minimum configuration that is required for NEA activation)
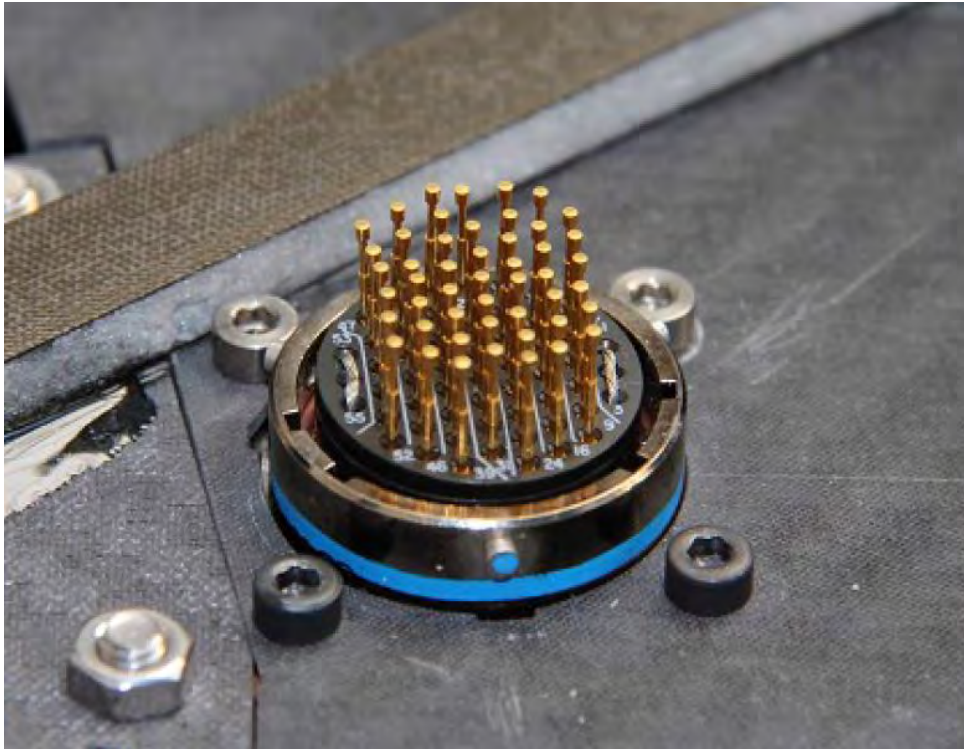
Figure 5.3.: MUSC equipped with 49 pins (flight configuration with full set)

insert on Lander side (push plate):
spring loaded test pin, customized for MPAE
supplier: PTR Messtechnik / D
specification : 1007−D1−0.3N(E)−Au−0.9C
            FK 063/97 dated 10 Mar 1998
material   :   copper beryllium
surface   :   Cu/Ni/Au
spring force nom. 0.30N at 2.4 mm compression

insert on MSS side :

custom pin
material phosphor bronze
surface: hard gold 0.002 mm
         (GALVATRONIC coating)
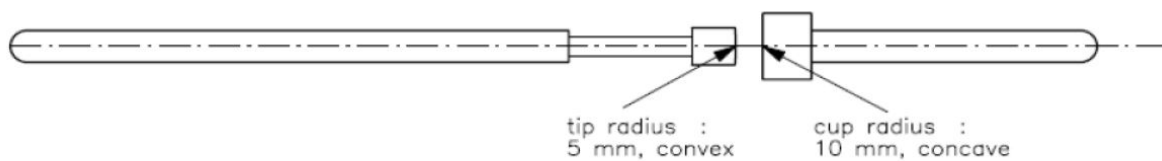   plus platinum 0.001 mm
by Collini−Flühmann / CH

tip radius :
5 mm, convex

cup radius :
10 mm, concave

Figure 5.4.: Schematic close up of a pin connection with its properties [4]

Bibliography

[1] *Kuninaka, H., Yano,H.: 2Hayabusa-2: A Carbonaceous Asteroid Sample Return Mission (2013)*

[2] *CNES, Hayabusa 2 spacecraft (Online)*
     http://smsc.cnes.fr/MASCOT/GP_sonde.htm (01.06.2014)

[3]   *Findlay,R., Ziach,C.: MASCOT Mobile Asteroid Surface Scout, System Design Definition: System, DLR, Bremen, (2013)*

[4] *Lange, M.: MASCOT Mobile Asteroid Surface Scout, System Design Definition: MESS, DLR, Bremen, (2013)*

[5] *Macdonald, M., Badescu, V.: The International Handbook of Space Technology.* (2014), Berlin Heidelberg: Springer-Verlag

[6] *ESA, Space Engineering, Mechanisms, Hold-Down and Separation Systems (Online)*
     http://www.esa.int/Our_Activities/Space_Engineering/Mechanisms/Hold-Down_and_Separation_Systems (16.10.2013)

[7] *NEA Electronics, Inc., Information Sheet/ Presentation* (2011)

[9] *ZARM Drop Tower Bremen User Manual,* Version: April 26, 2012

[10] *x-IMU User Manual 4.4* (2012)

A. Appendix

A.1. DTC Test Procedure

A.2. NEA_SSD9100-7

A.3. NEA2011 Mechanisms -GPK

A.4. ZARM_Users_Manual_0412

A.5. Buster8438_EN

A.6. MASCOT Separation Experiment No2 - Lessons Learned_v1.0